Mon. Not. R. Astron. Soc. **356,** 568–586 (2005) doi:10.1111/j.1365-2966.2004.08475.x

A deep *Chandra* survey of the Groth Strip – I. The X-ray data

K. Nandra,[1⋆] E. S. Laird,[1] K. Adelberger,[2] Jonathan P. Gardner,[3] R. F. Mushotzky,[4] J. Rhodes,[5] C. C. Steidel,[5] H. I. Teplitz[6] and K. A. Arnaud[4]

[1]*Astrophysics Group, Imperial College London, Blackett Laboratory, Prince Consort Road, London SW7 2AW*
[2]*Carnegie Observatories, 813 Santa Barbara Street, Pasadena, CA 91101, USA*
[3]*Laboratory for Astronomy and Solar Physics, Code 681, NASA's Goddard Space Flight Center, Greenbelt, MD 20771, USA*
[4]*Laboratory for High Energy Astrophysics, Code 660, NASA's Goddard Space Flight Center, Greenbelt, MD 20771, USA*
[5]*California Institute of Technology, Pasadena, CA 91125, USA*
[6]*Spitzer Science Center, California Institute of Technology, Pasadena, CA 91125, USA*

Accepted 2004 October 3. Received 2004 September 28; in original form 2004 July 16

ABSTRACT

We present the results of a 200-ks *Chandra* observation of part of the Groth Strip region, using the ACIS-I instrument. We present a relatively simple method for the detection of point sources and calculation of limiting sensitivities, which we argue is at least as sensitive and more self-consistent than previous methods presented in the literature. A total of 158 distinct X-ray sources are included in our point-source catalogue in the ACIS-I area. The number counts show a relative dearth of X-ray sources in this region. For example, at a flux limit of 10^{-15} erg cm^{-2} s^{-1}, around 20 per cent more soft-band sources are detected in the HDF-N and almost 50 per cent more in the ELAIS-N1 field, which we have analysed by the same method for comparison. We find, however, that these differences are consistent with Poisson variations at $<2\sigma$ significance, and therefore there is no evidence for cosmic variance based on these number counts alone. We determine the average spectra of the objects and find a marked difference between the soft-band-selected sources, which have $\Gamma = 1.9$ typical of unobscured active galactic nuclei (AGN), and the hard-band-selected sources, which have $\Gamma = 1.0$. Reassuringly, the sample as a whole has a mean spectrum of $\Gamma = 1.4 \pm 0.1$, the same as the X-ray background. None the less, our results imply that the fraction of sources with significant obscuration is only $\sim$25 per cent, much less than predicted by standard AGN population synthesis models. This is confirmed by direct spectral fitting, with only a handful of objects showing evidence for absorption. After accounting for absorption, all objects are consistent with a mean intrinsic spectrum of $\Gamma = 1.76 \pm 0.08$, very similar to local Seyfert galaxies. The survey area is distinguished by having outstanding multiwaveband coverage. Comparison with these observations and detailed discussion of the X-ray source properties will be presented in future papers.

Key words: surveys – galaxies: active – cosmology: observations – X-rays: diffuse background – X-rays: galaxies.

1 INTRODUCTION

Deep X-ray surveys, particularly with *Chandra*, have had enormous recent successes in resolving the X-ray background and shedding light on the nature and evolution of accretion power in galaxies (e.g. Mushotzky et al. 2000; Giacconi et al. 2001; Barger et al. 2001, 2002; Cowie et al. 2002, 2003). It should be borne in mind, however, that the number of fields for which both deep *Chandra* data and comprehensive supporting multiwavelength observations exist are relatively few. Aside from the deepest surveys in the *Hubble Deep Field* North (HDF-N) (Brandt et al. 2001a; Alexander et al. 2003, hereafter A03) and *Chandra Deep Field* South (CDF-S) (Tozzi et al. 2001; Giacconi et al. 2001, 2002; Rosati et al. 2002), only two other fields have been presented with a *Chandra* exposure in excess of 150 ks (Stern et al. 2002; Wang et al. 2004).

A particularly well-studied field in wavebands outside the X-ray is the Groth/Westphal Survey (GWS) area. The original 'Groth Strip' survey with the *Hubble Space Telescope* (*HST*; Groth et al. 1994) was complemented by a single deeper pointing, and further data have been obtained as part of the Canada–France Redshift Survey

⋆E-mail: k.nandra@imperial.ac.uk

(CFRS; Lilly et al. 1995). Comprehensive imaging with *HST*/ACS has now also been approved. The CFRS data have themselves been superseded by the Canada–France Deep Field (CFDF) survey (McCracken et al. 2001) and together they provide multiband imaging over much of the field. It has also been covered by deep optical imaging, and follow-up spectroscopy, in a Lyman break galaxy survey by Steidel et al. (2003). A further large optical spectroscopy effort is being undertaken as part of the DEEP and DEEP2 galaxy redshift surveys (Davis et al. 2003). SCUBA has observed a large area of the Groth Strip to deep limits for the Canada–UK Deep Submillimetre survey (Eales et al. 2000; Webb et al. 2003), and there is also coverage by the *Infrared Space Observatory* (*ISO*) (Flores et al. 1999) and in the radio (Fomalont et al. 1991). With a large number of on-going or future programmes for galaxy evolution in this field, e.g. DEEP2, *Spitzer*, Canada–France–Hawaii Telescope (CFHT), *HST*/ACS, and current interest in the connection between active galactic nuclei (AGN) and galaxy formation and evolution, deep X-ray data are clearly of great value.

Some X-ray data have been obtained in this field with *XMM* (Waskett et al. 2004; Miyaji et al. 2004). Here we report *Chandra* observations, which probe ∼5 times deeper in flux, obtained in a 200-ks exposure with the ACIS-I charge-coupled device (CCD) camera as prime instrument. This is currently the third deepest *Chandra* exposure, after the HDF-N and CDF-S.

2 OBSERVATIONS AND DATA REDUCTION

Chandra observed the GWS on three separate occasions between 2002 August 11 and 22, using ACIS-I as the prime instrument. The S2 and S3 chips of the ACIS-S array were also operating during the observation, but as these are far off-axis we do not consider the data further. The sequence number identifying the observations was 900144 and the three observation ID numbers (ObsIDs), along with some other basic observational information, are given in Table 1. The aim points of the observations were all very close to each other and close to the requested target position of $\alpha = 14{:}17{:}43.6$, $\delta = 52{:}28{:}41.2$. The latter is the position of the deep 'Westphal' pointing of *HST*/WFPC2 and the centre of the Lyman break galaxy survey field of Steidel et al. (2003). Our data reduction was performed using the CXC *Chandra* Interactive Analysis of Observations (CIAO) data analysis software, version 3.0.1, and the *Chandra* calibration data base (CALDB), version 2.23.

We first used the CIAO aspect calculator to check for known aspect errors in the three observations. No such offset needed to be applied to the observations. The expectation is therefore that the raw *Chandra* astrometry should be good to 1 arcsec. Charge Transfer Inefficiency corrections and updated gain maps were applied to the unfiltered (level 1) event files. We applied the standard screening criteria to the observations, choosing event grades 0, 2, 3, 4 and 6 (the standard '*ASCA*' grade set), applying the standard Good Time Intervals (GTIs) and removing flaring pixels and afterglow events. The filtered (level 2) event files were then energy-selected to permit events only in the 0.5–8 keV range. Outside this energy range the background is greatly elevated relative to any source signal.

During *Chandra* observations, it is known that there can be periods where the background is significantly higher compared to typical values. These background 'flares' are generally removed before analysis. To examine our observations for such effects, we initially performed a crude source detection on the 0.5–8 keV data for each ObsID separately using the CELLDETECT program, accepting all sources with signal-to-noise ratio (S/N) greater than 3. Excluding these detected sources, we generated background light curves for each observation. Light curves of these source-subtracted regions were analysed using the CIAO script ANALYZE_LTCRV.SL, which flags the periods where the background was $\pm 3\sigma$ from the mean value. Each of the three observations required filtering according to this prescription – approximately 5.3 ks were filtered from observation 3305, 5.7 ks from observation 4357 and 25 ks from observation 4365. The final filtered exposure time after this procedure was 158.5 ks: thus around 20 per cent of the data was lost due to apparent background flares using the ANALYZE_LTCRV.SL criteria. Examination of the light curves revealed that, rather than being primarily due to flaring, the bulk of the background rejection is due to a period of elevated, but relatively stable and well-behaved, background during observation 4365. The average background for the source-free regions was found to be ∼0.78 count s^{-1} for the first 60 ks of that ObsID, but it rose to an average of 1.38 count s^{-1} thereafter. Rather than adopt the ANALYZE_LTCRV.SL criteria blindly, we have also defined subjective background criteria to exclude noisy periods for each observation. These are shown in Table 1 and resulted in a final, total exposure time of 190.6 ks. We verified post hoc that inclusion of the additional ∼25 ks of data with elevated background in ObsID 4365 does indeed increase the sensitivity. For example, using WAVDETECT at a probability level of 10^{-7} results in 134 full-band sources using the full 190.6 ks (see below), whereas there were only 127 sources with the more strictly screened 158.5 ks exposure.

Before co-adding, the relative astrometry was improved by registering the observations to the coordinate frame of the observation 4357. This was done using bright (S/N > 4) sources within 6 arcmin of the aim point that were detected in each of the observations using the script ALIGN_EVT.PL (written by Tom Aldcroft). There were seven such sources common to observations 4357 and 3305, and 15 common to 4357 and 4365. The data sets were then co-added using the CIAO script MERGE_ALL. The resulting image was visually inspected to ensure that merging had not caused smearing or double peaking of point sources.

The 0.5–8 keV co-added level 2 event file was used to create images in a number of energy bands (Fig. 1). A specific issue in source detection is that of the upper energy bound. The HDF-N team has used an upper energy of 8 keV (e.g. Brandt et al. 2001a), with the CDF-S team choosing to restrict their search to below 7 keV (Giacconi et al. 2002). In our data set we found the latter to be more sensitive during source detection. More sources are detected in, for example, the 0.5–7 keV image compared to the 0.5–8 keV image, and no extra source is detected in, for example, the 4–8 keV image compared to the 4–7 keV image. We therefore restrict further analysis to the 0.5–7 keV (full band, FB), 0.5–2 keV (soft band, SB), 2–7 keV (hard band, HB) and 4–7 keV (ultra-hard band, UB) ranges. Source detection and other analysis proceeded with the images at the raw resolution of 0.492 arcsec $pixel^{-1}$.

Effective exposure maps were created for each of these bands using the MERGE_ALL script, which takes into account the effects such as vignetting and gaps between chips. The maps were created at a single energy representative of the mean energy of the photons in each band: 1 keV for the soft band, 2.5 keV for the full, 4 keV for the hard and 5.5 keV for the ultra-hard. These energies were determined post hoc by considering the average photon energy of the detected sources in each band. The exposure maps cover the ACIS-I chips 0, 1, 2 and 3 only, and are also unbinned.

3 DATA ANALYSIS

Numerous different techniques have been applied to *Chandra* deep surveys to find sources, assess their significance, and calculate their

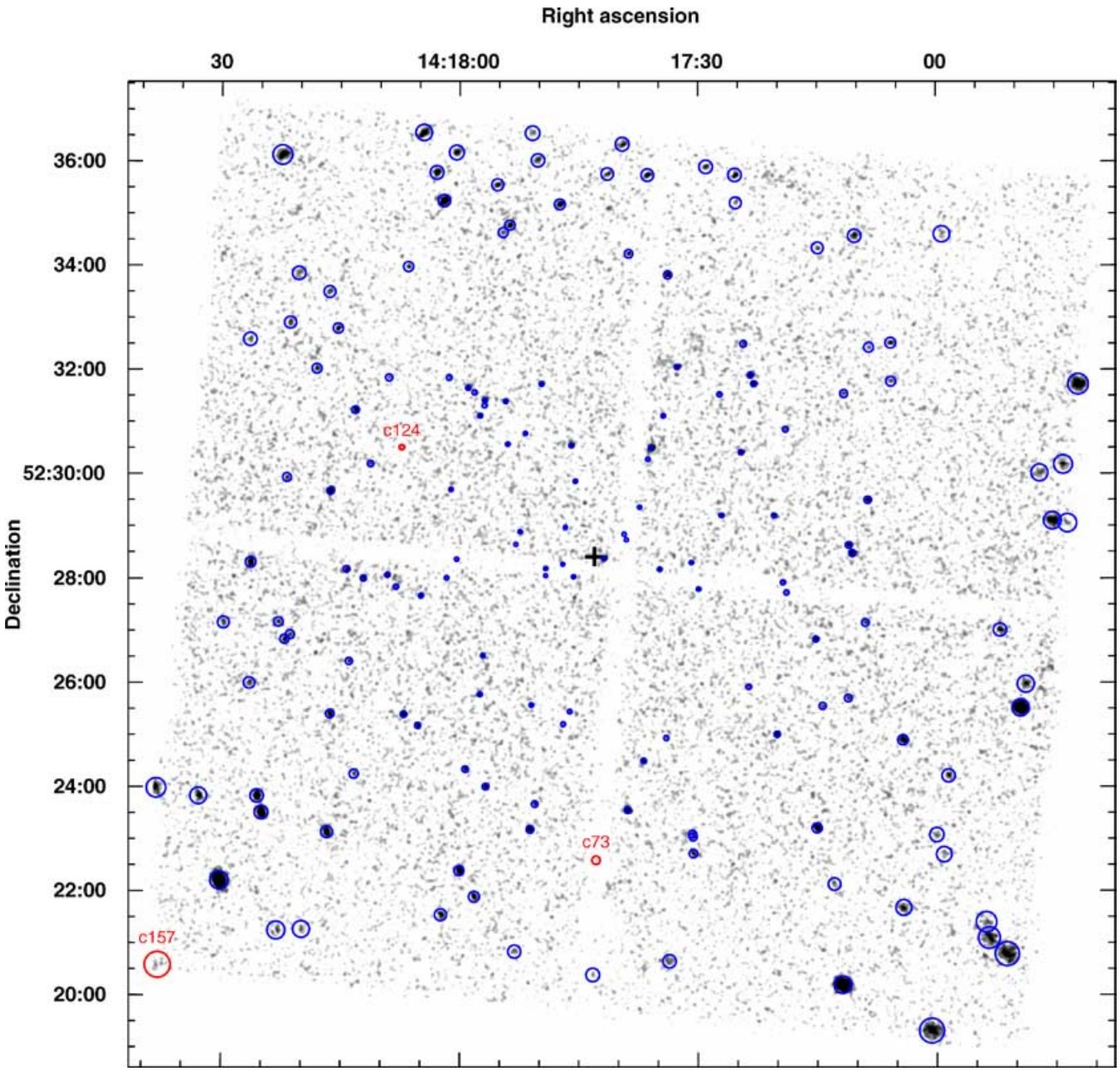

Figure 1. *Chandra* 0.5–7 keV image of the GWS. The image is approximately 18 arcmin on each side and has been smoothed with a Gaussian filter of 1.5 arcsec full width at half-maximum. The aimpoint is shown as a cross. The detected sources are marked as circles with radius equal to the 95 per cent PSF. The blue circles show detections in the full band, the red are soft band only (with catalogue name also marked). No object is detected exclusively in the hard band, though many are hard band detections without significant soft band counts.

Table 1. Log of *Chandra* observations. The columns are as follows: (1) sequence number of the observation; (2) date of beginning of observation; (3) time of beginning of observation; (4) nominal right ascension of satellite pointing; (5) nominal declination; (6) exposure time of unfiltered, level 1 events file (ks); (7) permitted background range (count s^{-1} – see text); (8) exposure time after GTI, background filtering, etc. (ks) – total good exposure was 190.6 ks.

Observation ID (1)	Date (UT) (2)	Time (UT) (3)	RA (J2000) (4)	Dec. (J2000) (5)	Raw exposure (6)	Background range (7)	Filtered exposure (8)
3305	2002-08-11	21:43:57	14:17:43.04	52:28:25.21	29.4	0.62–0.90	27.9
4357	2002-08-12	22:32:00	14:17:43.04	53:28:25.20	86.1	0.60–0.87	80.5
4365	2002-08-21	10:56:53	14:17:43.04	53:28:25.20	84.2	0.55–1.50	82.2

fluxes and source counts. These tasks are complicated by the fact that the ACIS-I background is very low, meaning that we have to deal with Poisson statistics. In addition, the point-source search algorithms often employed (e.g. WAVDETECT, Freeman et al. 2002; SExtractor, Bertin & Arnouts 1996) do not necessarily have well-defined sensitivities, making it difficult to define the flux limit as a function of area and/or assess the likely number of false sources in a catalogue. Generally, the tendency is to be conservative and try to minimize the latter. This has some advantages: in particular, it means that optical telescope time is not wasted following up 'spurious' sources. On the other hand, it runs the risk that many real sources may be missed. It is known that much information can be obtained about objects below these conservative thresholds, for example using fluctuation analysis (e.g. Miyaji & Griffiths 2002) or stacking (e.g. Brandt et al. 2001b; Nandra et al. 2002). In addition, different methods are often employed to identify likely significant sources, to determine their fluxes and errors, and to determine the sensitivity limits (see Section 4.1.1). This inconsistency has led us to develop our own point-source detection procedure.

3.1 Point-source detection

Our point-source detection method is as follows: First, WAVDETECT was run with a very low threshold probability of 10^{-4} on each of the four images, solely to identify positive fluctuations in the image that are candidate sources. A total of 1384 possible sources were identified in the four images, though many of these will have been detections in multiple bands. The numbers for each individual band are shown in Table 2. We then extracted counts, again in each image separately, from circular apertures centred both on the WAVDETECT-identified positions in that band and on a centroided position, with an extraction radius equal to 70 per cent encircled energy of the *Chandra* point spread function (PSF) at the appropriate mean energy of the image.

To calculate the PSF radii we used the MKPSF tool to create PSF images at the representative energy of each of the four bands, at the position of each candidate source, using the PSF information in the CALDB PSF library ACISI1998-11-052DPSF1N0002.FITS. We then extracted a radial profile of the PSF image by extracting counts from concentric circles centred on the source position out to a radius of 30 arcsec. Assuming all counts to be contained within the 30 arcsec radius, we then calculate by interpolation the radius at which 70 per cent of the counts are enclosed. This method can also be adapted to calculate the 90 per cent radius or other radii.

We note that, particularly very far off-axis in the hard energy band, the assumption that all counts are contained within 30 arcsec may not strictly be valid, but any error introduced by this is likely to be very small.

Background was determined locally from an annulus with inner radius equal to 1.5 times the 90 per cent PSF and outer radius 100 pixel greater than the inner radius. Detected sources from the WAVDETECT run were excluded from the background region, as were zero-exposure pixels. The background counts were then rescaled to the appropriate source region size, and by the ratio of the mean value of the exposure map in the source region to that in the background region. We can then calculate the Poisson probability that the source region would contain the number of counts it has based on the predicted background, apply a threshold, and determine what constitutes a detected source. This is performed for both the WAVDETECT and centroid position of each candidate. If only one passes the threshold, we adopt that position. If both do, we adopt the position that gives the larger number of counts.

We estimate the number of trials, and therefore the false source probability, by calculating the number of the PSF cells that fit into the total area of the image. This can be defined as

$$N_{\rm trial} = \sum_{i=1}^{N_{\rm pix}} \frac{a_{\rm pix}}{\pi r_{\rm PSF}^2},$$

where $a_{\rm pix}$ is the area of a pixel in arcseconds, $r_{\rm PSF}$ is the 70 per cent radius of the PSF in the same units, and the summation is over all the pixels $N_{\rm pix}$ in the image with non-zero exposure. For ultimate accuracy we would therefore have to calculate the PSF for >4 million pixels. The PSF calculation is time-consuming, however, and this would be prohibitive. As we have already calculated the PSF for a large number of representative positions in the image – for the candidate sources – to extract their counts, we instead assume that the PSF radius for each pixel is equal to the closest of these positions (the 'nearest-neighbour' PSF).

As the PSF is energy-dependent, $N_{\rm trial}$ depends on the energy band of the image. It ranges from ∼138 000 for the SB, which has the smallest PSF, to ∼94 000 for the UB, and the total of all four images was 4.6×10^5. The expected number of false sources is then $N_{\rm trial} \times p_{\rm thresh}$, where $p_{\rm thresh}$ is the threshold Poisson probability below which a source is considered a detection. We adopt $p_{\rm thresh} = 4 \times 10^{-6}$, at which level we expect approximately 0.5 false sources in each of the four images, and 1.8 in total. The latter matches the expected number of false sources using WAVDETECT with probability of 10^{-7}, which is a typical value used to produce point-source catalogues (e.g. A03; Wang et al. 2004). For a given $p_{\rm thresh}$, we expect fewer false sources with our method as we extract photons from cells with a fixed size and shape, unlike in WAVDETECT where the extraction region is of arbitrary geometry (Freeman et al. 2002).

3.2 Flux determination

The detection procedure described gives the total counts and background counts in the 70 per cent PSF region. To convert these for use in the $\log N - \log S$ function, we background-subtracted the counts, divided by the average value of the exposure map in the

Table 2. Number of detected sources. The columns are as follows: (1) detection method; (2) probability threshold; (3) merged sources; (4) full-band sources; (5) soft-band sources; (6) hard-band sources; (7) ultra-hard-band sources; (8) expected false sources per band for WAVDETECT (this is $N_{\rm pix} \times p_{\rm thresh}$) – the expected number of false sources for our method is discussed in the text.

Method (1)	$p_{\rm thresh}$ (2)	Merged (3)	FB (4)	SB (5)	HB (6)	UB (7)	$N_{\rm false}$ (8)
this paper	4×10^{-6}	158	155	121	100	44	1.8
WAVDETECT	1×10^{-7}	142	134	114	86	41	1.8
WAVDETECT	1×10^{-6}	170	151	132	101	48	17.7
WAVDETECT	1×10^{-5}	251	193	167	130	68	177
WAVDETECT	1×10^{-4}	894	379	414	317	274	1765

source detection cell, and corrected for counts falling outside the cell. This gives count rates corrected for the majority of the instrumental effects, such as the chip gaps, mirror vignetting and the ACIS quantum efficiency.

The CIAO exposure maps do not currently account for the degradation in the soft X-ray response of ACIS due to contamination (e.g. Marshall et al. 2004), the so-called 'ACISABS' correction. We determined this using the ACISABS model provided in the XSPEC spectral fitting package. The correction factors for the counts were found to be 8.8, 13.9 and 0.7 per cent for the FB, SB and HB respectively. The HB correction is therefore neglected, as is the negligible UB correction. We calculated the fluxes correcting for the Galactic $N_{\rm H}$ of 1.3×10^{20} cm^{-2} and assuming a spectrum of $\Gamma = 1.4$ for all the sources in all bands. This is the mean spectrum of the sources as deduced from analysis of the hardness ratios (see below). We converted the FB, HB and UB counts to fluxes in standard bands: 0.5–10, 2–10 and 5–10 keV, respectively. The SB flux is quoted for the same band as the counts, 0.5–2 keV.

For the source catalogue we want to merge sources detected in more than one band. The individual catalogues for the four bands were merged using a match radius of <2.5 arcsec for sources within 6 arcmin of the average aim point. Sources with larger off-axis angle were matched with a radius of 4 arcsec to reflect the larger PSF. Our analysis indicates that the mismatch probability using these radii, over the whole field, is less than 1 per cent. We assign the position in the full band to the object if it is detected in that band, as it contains most counts and hence the smallest statistical uncertainty. If undetected in the FB, we adopted consecutively the SB, HB and UB positions, although in practice no object was detected only in the HB or UB.

The 70 per cent PSF radius is appropriate for sensitive source detection, and we calculate the fluxes from this for the $\log N - \log S$ function because it maintains consistency between the source detection, the flux calculation and, as discussed below, the sensitivity calculation. It identifies positions in the image where there are significant sources of X-rays, and using a relatively small extraction radius optimizes the sensitivity for source detection. Given the photon-starved nature of the *Chandra* images, however, it is preferable to use a larger radius for source photometry, to increase the number of counts and improve constraints on the flux. For the source catalogue, after band merging, we therefore also extracted the counts using a circular aperture of radius equal to the point spread function 90 per cent encircled energy fraction (FB, HB, UB), or 95 per cent (SB; following A03) and subtracted background counts from a surrounding annulus as described above. Errors on the counts were determined according to the prescription of Gehrels (1986). We used his equation (7) to calculate the effective '1σ' upper bound on the counts and equation (14) for the corresponding lower bound.

As the source detection procedure has ensured a very high probability that a real X-ray source exists at the identified position, there is no need to apply the same thresholding to the cross-band matches as has been applied to the source detection. Indeed, all that needs to be ensured is that there are sufficient counts to give a meaningful estimate of the flux in that band. Following this merging process, and again only for the source catalogue, we have re-extracted the counts in all the bands based on the merged position. If the significance in the band exceeds the probability equivalent to 3σ for a one-tailed Gaussian distribution (1.3×10^{-3}), we calculate the counts, fluxes and errors in that band. Otherwise, we calculate the upper limit to the counts based on that same probability (i.e. the Poisson equivalent of a 3σ upper limit), by determining the number of counts that would produce a probability less than that value given the background.

3.3 Sensitivity map

The sensitivity map is needed in order to calculate, for example, the $\log N - \log S$ function for the field. The aperture extraction procedure also allows us to determine the sensitivity map for these observations easily, and in a manner consistent with the source detection.

In order to calculate the sensitivity as a function of the survey area, and therefore the $\log N - \log S$, we must calculate the count detection threshold for an extraction radius centred at every point in the image. Again, we have adopted the 'nearest-neighbour' approach. For each pixel, we determine the closest candidate source. We have already determined the PSF, and the expected background in the source cell for that position, with the latter simply needing to be rescaled to the mean exposure in the nominal source cell centred on each pixel. This rescaling will account, for example, for the change in sensitivity due to the chip gaps and chip edges. With the given background, we then determine how many counts would constitute a detection at $< 4 \times 10^{-6}$ Poisson probability, and convert that to the flux again using the mean exposure in the cell. We applied the ACISABS correction as above, and used a spectrum of $\Gamma = 1.4$ to convert to flux, just as for the detected sources.

4 RESULTS

4.1 Point-source catalogue

The point-source catalogue is shown in Table 3. At our adopted detection threshold of 4×10^{-6}, a total of 158 band-merged sources are detected, with the numbers detected in the individual bands shown in Table 2. No object is detected solely in the HB or UB, although ∼25 per cent of the sources remain undetected in the SB. These are candidate absorbed sources and we discuss their properties further below. In addition to the source counts, errors and detection probabilities in each band, the source catalogue also shows the fluxes in the standard bands, the off-axis angle and the hardness ratio, defined as

$$\frac{H - S}{H + S},$$

where H and S are the hard- and soft-band fluxes corrected to the on-axis value using the instrument map.

4.1.1 Comparison with WAVDETECT

The most common procedure for producing *Chandra* source catalogues it to use the wavelet-based algorithm WAVDETECT (Freeman et al. 2002). This algorithm is an extremely powerful and effective method of finding sources in *Chandra* images. There are, however, some disadvantages to its use compared with our adopted method. For example, as we discuss below, it is not straightforward to construct a sensitivity map from a WAVDETECT run. We first compare the efficiency of our source detection procedure to that of WAVDETECT.

We performed point-source searches using the CIAO WAVDETECT algorithm on the four GWS images (full, soft, hard and ultra-hard). Source detection was performed for each of the four bands using the appropriate exposure map, using wavelet scales of 1, $\sqrt{2}$, 2, $2\sqrt{2}$, 4, $4\sqrt{2}$, 8, $8\sqrt{2}$ and 16 pixels. The energy at which the PSF size was calculated in WAVDETECT was set at 1 keV (SB), 2.5 keV (FB), 4 keV (HB) and 5.5 keV (UB), just as in the creation of the exposure maps. Initially, the detection probability threshold was set at the typical value $p_{\rm thresh} = 10^{-7}$. The WAVDETECT documentation suggests that, as a rule of thumb, one would expect $p_{\rm thresh} \times N_{\rm pix}$ spurious sources

Table 3. *Chandra* GWS X-ray catalogue. The columns are as follows: (1) source catalogue number; (2) *Chandra* object name; (3) full-band (0.5–7 keV) counts; (4) soft-band (0.5–2 keV) counts; (5) hard-band (2–7 keV) counts; (6) ultra-hard-band (4–7 keV) counts; (7) 0.5–10 keV flux (all fluxes 10^{-15} erg cm^{-2} s^{-1}); (8) 0.5–2 keV flux; (9) 2–10 keV flux; (10) 5–10 keV flux; (11) lowest false detection probability found for the four bands – probabilities lower than 10^{-8} are not considered; (12) off-axis angle in arcminutes; (13) hardness ratio $= (H - S)/(H + S)$, where H and S are the 2–7 keV and 0.5–2 keV counts, corrected to on-axis values; (14) fshu = source detected at $< 4 \times 10^{-6}$ probability in this band, where the bands are full (f), soft (s), hard (h) and ultra-hard (u) – the first band quoted is the one with the lowest probability (i.e. that quoted in column 11).

Cat. No. (1)	CXO GWS (2000) (2)	FB counts (3)	SB counts (4)	HB counts (5)	UB counts (6)	0.5–10.0 flux (7)	0.5–2.0 flux (8)	2–10 flux (9)	5–10 flux (10)	$p_{\min}$ (11)	OAA (arcmin) (12)	HR (13)	Flags (14)
c1	J141642.1+523142	$424.5^{+22.4}_{-21.4}$	$310.1^{+19.0}_{-18.0}$	$117.8^{+12.8}_{-11.8}$	$36.9^{+8.1}_{-7.0}$	$41.00^{+2.00}_{-1.90}$	$12.00^{+0.70}_{-0.66}$	$25.00^{+2.40}_{-2.20}$	$17.00^{+2.80}_{-2.40}$	$10^{-8.0}$	9.90	−0.4	fshu
c2	J141643.5+522902	$26.8^{+8.1}_{-7.0}$	$18.1^{+6.3}_{-5.2}$	$10.2^{+6.2}_{-5.1}$	< 12.13	$2.90^{+0.47}_{-0.41}$	$0.78^{+0.18}_{-0.15}$	$2.50^{+0.59}_{-0.49}$	< 6.00	$10^{-6.5}$	9.10	−0.3	f
c3	J141644.0+523010	$66.0^{+11.1}_{-10.0}$	$38.8^{+8.4}_{-7.3}$	$27.6^{+8.2}_{-7.1}$	< 13.96	$4.80^{+0.53}_{-0.48}$	$1.10^{+0.17}_{-0.15}$	$4.50^{+0.72}_{-0.63}$	< 4.60	$10^{-8.0}$	9.20	−0.2	fsh
c4	J141645.3+522905	$210.0^{+16.6}_{-15.6}$	$148.2^{+13.8}_{-12.7}$	$64.0^{+10.4}_{-9.3}$	< 13.97	$15.00^{+1.00}_{-0.94}$	$4.10^{+0.34}_{-0.32}$	$10.00^{+1.20}_{-1.10}$	< 4.40	$10^{-8.0}$	8.80	−0.4	fsh
c5	J141646.9+523000	$43.1^{+9.6}_{-8.5}$	$33.8^{+7.9}_{-6.8}$	< 15.97	< 13.25	$2.90^{+0.39}_{-0.34}$	$0.90^{+0.15}_{-0.13}$	< 2.30	< 4.00	$10^{-8.0}$	8.70	−1.0	fs
c6	J141648.8+522558	$76.0^{+11.2}_{-10.2}$	$54.3^{+9.3}_{-8.2}$	$23.1^{+7.5}_{-6.4}$	< 11.46	$7.10^{+0.77}_{-0.70}$	$2.00^{+0.27}_{-0.24}$	$4.90^{+0.89}_{-0.76}$	< 4.90	$10^{-8.0}$	8.60	−0.4	fs
c7	J141649.4+522530	$896.1^{+31.4}_{-30.4}$	$636.5^{+26.5}_{-25.5}$	$278.2^{+18.2}_{-17.2}$	$75.3^{+10.3}_{-9.2}$	$87.00^{+2.90}_{-2.90}$	$24.00^{+0.98}_{-0.94}$	$61.00^{+3.70}_{-3.50}$	$35.00^{+4.20}_{-3.80}$	$10^{-8.0}$	8.70	−0.4	fshu
c8	J141651.2+522047	$355.8^{+21.2}_{-20.2}$	$264.0^{+18.0}_{-17.0}$	$105.4^{+12.7}_{-11.7}$	$27.2^{+7.8}_{-6.7}$	$30.00^{+1.50}_{-1.50}$	$8.60^{+0.54}_{-0.51}$	$20.00^{+1.80}_{-1.70}$	$11.00^{+2.00}_{-1.70}$	$10^{-8.0}$	11.00	−0.4	fsh
c9	J141652.0+522700	$57.4^{+9.8}_{-8.7}$	$34.9^{+7.6}_{-6.5}$	$25.4^{+7.2}_{-6.1}$	< 10.93	$4.00^{+0.52}_{-0.46}$	$0.96^{+0.17}_{-0.15}$	$4.00^{+0.77}_{-0.65}$	< 3.50	$10^{-8.0}$	7.90	−0.1	fsh
c10	J141653.4+522105	$200.5^{+16.5}_{-15.5}$	$119.3^{+12.8}_{-11.8}$	$82.8^{+11.4}_{-10.4}$	$17.7^{+6.7}_{-5.6}$	$17.00^{+1.20}_{-1.10}$	$4.00^{+0.37}_{-0.34}$	$16.00^{+1.70}_{-1.50}$	$7.50^{+1.60}_{-1.30}$	$10^{-8.0}$	10.50	−0.2	fsh
c11	J141653.8+522123	$53.8^{+10.7}_{-9.7}$	< 15.49	$44.2^{+9.4}_{-8.3}$	$18.8^{+6.9}_{-5.8}$	$4.10^{+0.47}_{-0.43}$	< 0.47	$7.70^{+1.00}_{-0.92}$	$7.20^{+1.50}_{-1.20}$	$10^{-8.0}$	10.30	1.0	fhu
c12	J141658.5+522412	$40.8^{+8.5}_{-7.5}$	$20.3^{+6.3}_{-5.2}$	$21.5^{+6.7}_{-5.6}$	< 9.53	$3.10^{+0.47}_{-0.41}$	$0.60^{+0.14}_{-0.11}$	$3.60^{+0.76}_{-0.64}$	< 3.20	$10^{-8.0}$	8.00	0.1	fsh
c13	J141659.1+522241	$19.3^{+7.3}_{-6.2}$	$4.1^{+4.7}_{-3.5}$	$14.6^{+6.4}_{-5.3}$	< 11.17	$1.40^{+0.27}_{-0.23}$	$0.12^{+0.04}_{-0.03}$	$2.50^{+0.56}_{-0.46}$	< 3.80	$10^{-5.8}$	8.80	0.6	f
c14	J141659.2+523436	$20.3^{+7.5}_{-6.4}$	< 11.94	$16.6^{+6.6}_{-5.5}$	$9.0^{+5.3}_{-4.2}$	$1.40^{+0.25}_{-0.21}$	< 0.32	$2.60^{+0.55}_{-0.46}$	$2.90^{+0.87}_{-0.68}$	$10^{-5.9}$	9.10	1.0	fh
c15	J141700.0+522304	$20.9^{+7.2}_{-6.1}$	< 11.05	$15.2^{+6.3}_{-5.2}$	< 10.35	$1.60^{+0.30}_{-0.25}$	< 0.33	$2.60^{+0.60}_{-0.49}$	< 3.50	$10^{-8.0}$	8.50	1.0	fh
c16	J141700.6+521918	$365.6^{+21.4}_{-20.4}$	$309.1^{+19.2}_{-18.2}$	$59.7^{+10.7}_{-9.7}$	$21.3^{+7.4}_{-6.3}$	$29.00^{+1.50}_{-1.40}$	$9.70^{+0.56}_{-0.53}$	$11.00^{+1.20}_{-1.10}$	$8.40^{+1.50}_{-1.30}$	$10^{-8.0}$	11.20	−0.7	fsh
c17	J141704.1+522140	$69.4^{+10.6}_{-9.6}$	$21.9^{+6.7}_{-5.6}$	$47.5^{+9.0}_{-7.9}$	$17.4^{+6.3}_{-5.2}$	$4.90^{+0.56}_{-0.51}$	$0.60^{+0.13}_{-0.11}$	$7.40^{+1.10}_{-0.93}$	$5.80^{+1.30}_{-1.10}$	$10^{-8.0}$	9.00	0.4	fshu
c18	J141704.2+522453	$107.2^{+11.9}_{-10.8}$	$12.2^{+5.2}_{-4.1}$	$98.5^{+11.3}_{-10.2}$	$48.7^{+8.3}_{-7.2}$	$7.20^{+0.72}_{-0.66}$	$0.32^{+0.10}_{-0.08}$	$15.00^{+1.60}_{-1.40}$	$15.00^{+2.30}_{-2.00}$	$10^{-8.0}$	6.90	0.8	fshu
c19	J141705.7+523146	$16.9^{+6.0}_{-4.9}$	< 7.50	$13.3^{+5.3}_{-4.2}$	< 6.97	$1.30^{+0.33}_{-0.26}$	< 0.23	$2.30^{+0.67}_{-0.53}$	< 2.30	$10^{-8.0}$	6.60	1.0	fh
c20	J141705.7+523230	$35.4^{+7.7}_{-6.6}$	$27.1^{+6.6}_{-5.5}$	$9.0^{+5.0}_{-3.8}$	< 7.92	$2.60^{+0.46}_{-0.39}$	$0.79^{+0.17}_{-0.14}$	$1.50^{+0.49}_{-0.37}$	< 2.50	$10^{-8.0}$	7.00	−0.5	fs
c21	J141708.4+523225	$13.4^{+5.7}_{-4.5}$	$10.8^{+4.8}_{-3.7}$	< 8.75	< 7.64	$1.00^{+0.27}_{-0.22}$	$0.31^{+0.11}_{-0.08}$	< 1.40	< 2.40	$10^{-8.0}$	6.60	−1.0	sf
c22	J141708.6+522929	$39.0^{+7.6}_{-6.5}$	$29.0^{+6.6}_{-5.5}$	$11.2^{+4.8}_{-3.7}$	< 6.08	$2.80^{+0.49}_{-0.42}$	$0.81^{+0.17}_{-0.14}$	$1.80^{+0.61}_{-0.46}$	< 1.80	$10^{-8.0}$	5.40	−0.4	fs
c23	J141708.9+522708	$15.8^{+5.7}_{-4.5}$	$11.7^{+4.8}_{-3.7}$	$8.3^{+4.6}_{-3.4}$	< 7.40	$1.00^{+0.28}_{-0.22}$	$0.30^{+0.10}_{-0.08}$	$1.20^{+0.46}_{-0.34}$	< 2.00	$10^{-8.0}$	5.30	−0.2	f
c24	J141710.2+523433	$48.2^{+9.1}_{-8.0}$	$21.0^{+6.4}_{-5.3}$	$29.0^{+7.3}_{-6.2}$	$10.6^{+5.2}_{-4.1}$	$3.20^{+0.46}_{-0.40}$	$0.55^{+0.12}_{-0.10}$	$4.30^{+0.81}_{-0.69}$	$3.30^{+1.00}_{-0.79}$	$10^{-8.0}$	7.90	0.2	fshu
c25	J141710.6+522828	$119.4^{+12.1}_{-11.1}$	$92.4^{+10.7}_{-9.7}$	$29.5^{+6.7}_{-5.6}$	< 6.32	$8.50^{+0.84}_{-0.76}$	$2.60^{+0.30}_{-0.27}$	$4.60^{+0.98}_{-0.82}$	< 1.90	$10^{-8.0}$	4.90	−0.5	fsh
c26	J141711.0+522837	$40.7^{+7.7}_{-6.6}$	$28.5^{+6.6}_{-5.4}$	$14.7^{+5.2}_{-4.1}$	$9.4^{+4.4}_{-3.3}$	$3.00^{+0.52}_{-0.45}$	$0.82^{+0.18}_{-0.15}$	$2.40^{+0.73}_{-0.57}$	$3.00^{+1.20}_{-0.90}$	$10^{-8.0}$	4.90	−0.3	fshu
c27	J141711.1+522541	$19.2^{+6.0}_{-4.9}$	$19.8^{+5.8}_{-4.7}$	< 7.63	< 6.62	$1.30^{+0.33}_{-0.27}$	$0.54^{+0.14}_{-0.11}$	< 1.10	< 2.00	$10^{-8.0}$	5.60	−1.0	fs
c28	J141711.6+523132	$17.5^{+5.9}_{-4.8}$	$16.2^{+5.4}_{-4.3}$	< 8.27	< 6.47	$1.10^{+0.29}_{-0.23}$	$0.41^{+0.12}_{-0.09}$	< 1.10	< 1.70	$10^{-8.0}$	5.70	−1.0	sf
c29	J141711.8+522011	$950.9^{+32.3}_{-31.2}$	$720.2^{+28.1}_{-27.0}$	$268.9^{+17.9}_{-16.9}$	$91.8^{+11.1}_{-10.1}$	$68.00^{+2.20}_{-2.20}$	$20.00^{+0.77}_{-0.74}$	$43.00^{+2.70}_{-2.50}$	$31.00^{+3.40}_{-3.10}$	$10^{-8.0}$	9.50	−0.4	fshu
c30	J141712.9+522207	$17.6^{+6.6}_{-5.4}$	$5.3^{+4.4}_{-3.3}$	$12.3^{+5.7}_{-4.5}$	< 9.54	$1.30^{+0.28}_{-0.24}$	$0.15^{+0.06}_{-0.05}$	$2.00^{+0.54}_{-0.44}$	< 3.10	$10^{-8.0}$	7.80	0.4	f

Table 3 – *continued*

Cat. No. (1)	CXO GWS (2000) (2)	FB counts (3)	SB counts (4)	HB counts (5)	UB counts (6)	0.5–10.0 flux (7)	0.5–2.0 flux (8)	2–10 flux (9)	5–10 flux (10)	$p_{\rm min}$ (11)	OAA (arcmin) (12)	HR (13)	Flags (14)
c31	J141714.3+522532	$14.8^{+5.4}_{-4.3}$	$12.1^{+4.8}_{-3.7}$	< 7.17	< 6.09	$0.96^{+0.28}_{-0.22}$	$0.31^{+0.11}_{-0.08}$	< 0.97	< 1.60	$10^{-8.0}$	5.20	−1.0	sf
c32	J141714.9+523420	$14.4^{+6.2}_{-5.1}$	< 9.05	$10.5^{+5.3}_{-4.2}$	< 8.46	$0.96^{+0.23}_{-0.19}$	< 0.24	$1.60^{+0.46}_{-0.36}$	< 2.40	$10^{-7.2}$	7.30	1.0	fh
c33	J141715.0+522312	$149.0^{+13.6}_{-12.6}$	$112.8^{+11.9}_{-10.8}$	$39.9^{+7.8}_{-6.8}$	$10.2^{+4.8}_{-3.7}$	$10.00^{+0.90}_{-0.83}$	$3.10^{+0.32}_{-0.29}$	$6.20^{+1.10}_{-0.91}$	$3.20^{+1.10}_{-0.84}$	$10^{-8.0}$	6.70	−0.5	fshu
c34	J141715.2+522649	$61.8^{+9.1}_{-8.0}$	$19.7^{+5.7}_{-4.5}$	$41.9^{+7.7}_{-6.6}$	$11.5^{+4.7}_{-3.5}$	$4.30^{+0.60}_{-0.53}$	$0.54^{+0.14}_{-0.12}$	$6.40^{+1.10}_{-0.96}$	$3.50^{+1.30}_{-0.95}$	$10^{-8.0}$	4.50	0.4	fshu
c35	J141718.8+522743	$7.1^{+4.0}_{-2.8}$	$6.6^{+3.8}_{-2.6}$	< 4.33	< 3.54	$1.10^{+0.53}_{-0.37}$	$0.39^{+0.21}_{-0.14}$	< 1.40	< 2.20	$10^{-6.0}$	3.70	−1.0	f
c36	J141719.0+523051	$11.4^{+4.8}_{-3.7}$	$7.8^{+4.1}_{-2.9}$	< 6.11	< 5.68	$0.72^{+0.25}_{-0.19}$	$0.19^{+0.09}_{-0.06}$	< 0.80	< 1.50	$10^{-8.0}$	4.40	−1.0	fs
c37	J141719.3+522755	$14.7^{+5.1}_{-4.0}$	$9.4^{+4.3}_{-3.1}$	$5.0^{+3.6}_{-2.4}$	< 4.37	$1.50^{+0.47}_{-0.36}$	$0.37^{+0.16}_{-0.12}$	$1.10^{+0.67}_{-0.44}$	< 1.80	$10^{-8.0}$	3.60	−0.3	fs
c38	J141720.0+522500	$47.6^{+8.2}_{-7.1}$	$27.5^{+6.4}_{-5.3}$	$22.6^{+6.1}_{-5.0}$	$4.3^{+3.6}_{-2.4}$	$3.10^{+0.49}_{-0.43}$	$0.70^{+0.16}_{-0.13}$	$3.20^{+0.78}_{-0.64}$	$1.20^{+0.73}_{-0.48}$	$10^{-8.0}$	4.90	−0.1	fsh
c39	J141720.4+522911	$21.4^{+5.9}_{-4.8}$	$18.2^{+5.4}_{-4.3}$	< 5.75	< 5.04	$1.30^{+0.34}_{-0.28}$	$0.45^{+0.13}_{-0.10}$	< 0.75	< 1.30	$10^{-8.0}$	3.50	−1.0	fs
c40	J141722.9+523143	$46.3^{+8.1}_{-7.0}$	$35.7^{+7.1}_{-6.1}$	$11.1^{+4.7}_{-3.5}$	< 5.70	$3.00^{+0.50}_{-0.43}$	$0.93^{+0.18}_{-0.15}$	$1.60^{+0.58}_{-0.44}$	< 1.50	$10^{-8.0}$	4.50	−0.5	fsh
c41	J141723.4+523153	$216.3^{+15.8}_{-14.8}$	$176.7^{+14.4}_{-13.3}$	$41.1^{+7.6}_{-6.5}$	$9.7^{+4.4}_{-3.3}$	$15.00^{+1.10}_{-0.99}$	$4.70^{+0.38}_{-0.35}$	$6.10^{+1.10}_{-0.93}$	$2.80^{+1.10}_{-0.84}$	$10^{-8.0}$	4.60	−0.6	fshu
c42	J141723.6+522555	$13.0^{+5.0}_{-3.8}$	$4.1^{+3.4}_{-2.2}$	$9.7^{+4.4}_{-3.3}$	< 4.96	$0.83^{+0.27}_{-0.21}$	$0.10^{+0.07}_{-0.04}$	$1.30^{+0.54}_{-0.40}$	< 1.30	$10^{-8.0}$	3.90	0.4	fh
c43	J141724.3+523229	$14.4^{+5.3}_{-4.2}$	$12.2^{+4.8}_{-3.7}$	< 7.38	< 6.16	$0.92^{+0.27}_{-0.21}$	$0.31^{+0.11}_{-0.08}$	< 0.98	< 1.60	$10^{-8.0}$	5.00	−1.0	fs
c44	J141724.6+523024	$565.5^{+24.8}_{-23.8}$	$383.3^{+20.6}_{-19.6}$	$187.9^{+14.8}_{-13.7}$	$56.1^{+8.6}_{-7.5}$	$36.00^{+1.60}_{-1.50}$	$9.60^{+0.52}_{-0.49}$	$26.00^{+2.00}_{-1.90}$	$15.00^{+2.30}_{-2.00}$	$10^{-8.0}$	3.40	−0.3	fshu
c45	J141725.2+523512	$12.6^{+6.0}_{-4.9}$	$9.2^{+5.0}_{-3.8}$	< 10.57	< 8.60	$0.84^{+0.21}_{-0.17}$	$0.24^{+0.08}_{-0.06}$	< 1.50	< 2.50	$10^{-5.4}$	7.30	−1.0	f
c46	J141725.3+523544	$51.2^{+9.2}_{-8.1}$	$27.2^{+7.0}_{-5.9}$	$21.5^{+6.6}_{-5.5}$	< 9.41	$3.50^{+0.48}_{-0.42}$	$0.72^{+0.14}_{-0.12}$	$3.20^{+0.69}_{-0.58}$	< 2.80	$10^{-8.0}$	7.80	−0.1	fsh
c47	J141727.0+522911	$85.1^{+10.3}_{-9.2}$	$62.5^{+9.0}_{-7.9}$	$22.3^{+5.9}_{-4.8}$	$8.4^{+4.1}_{-2.9}$	$5.20^{+0.63}_{-0.56}$	$1.50^{+0.22}_{-0.19}$	$3.00^{+0.76}_{-0.62}$	$2.20^{+0.99}_{-0.70}$	$10^{-8.0}$	2.60	−0.5	fshu
c48	J141727.3+523131	$11.9^{+4.8}_{-3.7}$	$7.9^{+4.1}_{-2.9}$	$6.5^{+4.0}_{-2.8}$	< 4.93	$0.75^{+0.26}_{-0.20}$	$0.20^{+0.09}_{-0.06}$	$0.90^{+0.44}_{-0.31}$	< 1.20	$10^{-8.0}$	3.90	−0.1	fs
c49	J141729.0+523553	$32.7^{+7.8}_{-6.8}$	$21.8^{+6.4}_{-5.3}$	$11.3^{+5.6}_{-4.4}$	< 9.43	$2.40^{+0.41}_{-0.35}$	$0.63^{+0.14}_{-0.12}$	$1.80^{+0.51}_{-0.41}$	< 3.00	$10^{-8.0}$	7.80	−0.3	fs
c50	J141729.9+522747	$87.5^{+10.4}_{-9.4}$	$60.8^{+8.9}_{-7.8}$	$28.6^{+6.4}_{-5.3}$	$7.7^{+4.0}_{-2.8}$	$9.20^{+1.10}_{-0.98}$	$2.50^{+0.37}_{-0.32}$	$6.60^{+1.50}_{-1.20}$	$3.40^{+1.70}_{-1.20}$	$10^{-8.0}$	2.10	−0.3	fshu
c51	J141730.6+522242	$35.0^{+7.5}_{-6.4}$	$25.1^{+6.4}_{-5.3}$	$10.7^{+5.0}_{-3.8}$	< 7.18	$2.30^{+0.43}_{-0.36}$	$0.66^{+0.15}_{-0.12}$	$1.60^{+0.52}_{-0.40}$	< 2.00	$10^{-8.0}$	6.00	−0.4	fs
c52	J141730.6+522302	$20.9^{+6.2}_{-5.1}$	$17.7^{+5.6}_{-4.4}$	< 7.43	< 6.63	$1.40^{+0.33}_{-0.27}$	$0.46^{+0.13}_{-0.10}$	< 1.00	< 1.80	$10^{-8.0}$	5.70	−1.0	fs
c53	J141730.7+522305	$21.2^{+6.2}_{-5.1}$	$16.6^{+5.4}_{-4.3}$	$6.4^{+4.3}_{-3.1}$	< 6.76	$1.40^{+0.33}_{-0.27}$	$0.43^{+0.12}_{-0.10}$	$0.93^{+0.40}_{-0.29}$	< 1.90	$10^{-8.0}$	5.60	−0.4	fs
c54	J141730.8+522818	$16.2^{+5.2}_{-4.1}$	< 3.68	$12.4^{+4.7}_{-3.5}$	$5.4^{+3.6}_{-2.4}$	$0.99^{+0.30}_{-0.24}$	< 0.09	$1.70^{+0.60}_{-0.45}$	$1.40^{+0.83}_{-0.55}$	$10^{-8.0}$	1.90	1.0	fh
c55	J141732.6+523202	$158.7^{+13.7}_{-12.7}$	$103.8^{+11.3}_{-10.2}$	$59.5^{+8.9}_{-7.8}$	$19.0^{+5.6}_{-4.4}$	$11.00^{+0.93}_{-0.86}$	$2.80^{+0.30}_{-0.27}$	$9.00^{+1.30}_{-1.10}$	$5.60^{+1.50}_{-1.20}$	$10^{-8.0}$	4.00	−0.3	fshu
c56	J141733.6+522038	$41.5^{+8.5}_{-7.5}$	< 9.55	$35.1^{+7.8}_{-6.7}$	$18.4^{+6.0}_{-4.9}$	$2.90^{+0.44}_{-0.38}$	< 0.26	$5.40^{+0.93}_{-0.80}$	$5.90^{+1.50}_{-1.20}$	$10^{-8.0}$	7.90	1.0	fh
c57	J141733.8+523349	$64.6^{+9.4}_{-8.3}$	$32.2^{+7.0}_{-5.9}$	$32.2^{+7.1}_{-6.0}$	$11.5^{+4.8}_{-3.7}$	$4.20^{+0.56}_{-0.50}$	$0.82^{+0.16}_{-0.14}$	$4.60^{+0.90}_{-0.76}$	$3.30^{+1.10}_{-0.86}$	$10^{-8.0}$	5.60	0.0	fshu
c58	J141734.0+522456	$8.1^{+4.3}_{-3.1}$	< 5.15	$7.5^{+4.1}_{-2.9}$	$4.0^{+3.4}_{-2.2}$	$0.51^{+0.22}_{-0.16}$	< 0.13	$1.00^{+0.48}_{-0.34}$	$1.10^{+0.74}_{-0.47}$	$10^{-6.1}$	3.70	1.0	fh
c59	J141734.4+523106	$33.7^{+7.0}_{-5.9}$	$23.2^{+6.0}_{-4.9}$	$10.1^{+4.4}_{-3.3}$	< 4.29	$2.20^{+0.44}_{-0.38}$	$0.61^{+0.15}_{-0.12}$	$1.50^{+0.59}_{-0.43}$	< 1.10	$10^{-8.0}$	3.00	−0.4	fsh
c60	J141734.8+522810	$228.4^{+16.2}_{-15.1}$	$170.8^{+14.1}_{-13.1}$	$63.6^{+9.1}_{-8.0}$	$16.6^{+5.2}_{-4.1}$	$21.00^{+1.50}_{-1.40}$	$6.30^{+0.52}_{-0.48}$	$13.00^{+1.80}_{-1.60}$	$6.50^{+2.00}_{-1.60}$	$10^{-8.0}$	1.30	−0.4	fshu
c61	J141735.9+523029	$2674.1^{+52.7}_{-51.7}$	$1951.5^{+45.2}_{-44.2}$	$760.3^{+28.6}_{-27.6}$	$239.3^{+16.5}_{-15.5}$	$160.00^{+3.20}_{-3.20}$	$47.00^{+1.10}_{-1.10}$	$100.00^{+3.80}_{-3.70}$	$62.00^{+4.20}_{-4.00}$	$10^{-8.0}$	2.30	−0.4	fshu
c62	J141736.3+523016	$9.9^{+4.4}_{-3.3}$	$6.5^{+3.8}_{-2.6}$	$3.3^{+3.2}_{-1.9}$	< 4.34	$0.60^{+0.24}_{-0.18}$	$0.16^{+0.09}_{-0.06}$	$0.44^{+0.35}_{-0.21}$	< 1.10	$10^{-6.4}$	2.10	−0.3	f

Table 3 – *continued*

Cat. No. (1)	CXO GWS (2000) (2)	FB counts (3)	SB counts (4)	HB counts (5)	UB counts (6)	0.5–10.0 flux (7)	0.5–2.0 flux (8)	2–10 flux (9)	5–10 flux (10)	$p_{\min}$ (11)	OAA (arcmin) (12)	HR (13)	Flags (14)
c63	J141736.3+523544	$53.4^{+9.1}_{-8.0}$	$43.5^{+8.1}_{-7.0}$	$12.2^{+5.6}_{-4.4}$	< 9.22	$4.00^{+0.56}_{-0.49}$	$1.30^{+0.21}_{-0.18}$	$2.10^{+0.57}_{-0.45}$	< 3.10	$10^{-8.0}$	7.40	−0.6	fs
c64	J141736.8+522429	$93.8^{+10.8}_{-9.8}$	$69.0^{+9.4}_{-8.3}$	$26.4^{+6.4}_{-5.3}$	$7.9^{+4.1}_{-2.9}$	$6.00^{+0.68}_{-0.61}$	$1.80^{+0.24}_{-0.21}$	$3.70^{+0.84}_{-0.70}$	$2.20^{+0.99}_{-0.71}$	$10^{-8.0}$	4.00	−0.4	fshu
c65	J141737.3+522921	$13.4^{+4.8}_{-3.7}$	< 2.79	$13.6^{+4.8}_{-3.7}$	$4.6^{+3.4}_{-2.2}$	$1.10^{+0.37}_{-0.28}$	< 0.09	$2.40^{+0.82}_{-0.62}$	$1.50^{+1.00}_{-0.66}$	$10^{-8.0}$	1.30	1.0	fhu
c66	J141738.7+523413	$23.0^{+6.4}_{-5.3}$	$16.4^{+5.4}_{-4.3}$	$6.7^{+4.4}_{-3.3}$	< 7.32	$1.50^{+0.34}_{-0.28}$	$0.42^{+0.12}_{-0.10}$	$0.98^{+0.39}_{-0.29}$	< 2.10	$10^{-8.0}$	5.80	−0.4	fs
c67	J141738.8+522332	$311.6^{+18.8}_{-17.7}$	$232.4^{+16.3}_{-15.3}$	$87.6^{+10.5}_{-9.5}$	$27.4^{+6.4}_{-5.3}$	$20.00^{+1.20}_{-1.20}$	$6.00^{+0.42}_{-0.39}$	$13.00^{+1.50}_{-1.30}$	$7.70^{+1.70}_{-1.40}$	$10^{-8.0}$	4.90	−0.4	fshu
c68	J141739.0+522843	$4.7^{+3.4}_{-2.2}$	$3.8^{+3.2}_{-1.9}$	< 3.76	< 3.78	$0.66^{+0.45}_{-0.29}$	$0.21^{+0.17}_{-0.10}$	< 1.10	< 2.20	$10^{-6.5}$	0.70	−1.0	fs
c69	J141739.3+522850	$4.7^{+3.4}_{-2.2}$	< 2.86	$4.8^{+3.4}_{-2.2}$	$3.8^{+3.2}_{-1.9}$	$0.77^{+0.52}_{-0.33}$	< 0.18	$1.70^{+1.20}_{-0.75}$	$2.70^{+2.10}_{-1.30}$	$10^{-7.2}$	0.70	1.0	hf
c70	J141739.5+523619	$49.5^{+9.1}_{-8.0}$	$35.0^{+7.5}_{-6.4}$	$12.5^{+5.9}_{-4.8}$	< 9.57	$3.40^{+0.47}_{-0.42}$	$0.94^{+0.17}_{-0.14}$	$1.90^{+0.49}_{-0.40}$	< 2.90	$10^{-8.0}$	7.90	−0.5	fs
c71	J141741.4+523545	$30.9^{+7.7}_{-6.6}$	$10.9^{+5.2}_{-4.1}$	$19.3^{+6.4}_{-5.3}$	< 9.62	$2.10^{+0.36}_{-0.31}$	$0.29^{+0.09}_{-0.07}$	$2.90^{+0.66}_{-0.55}$	< 2.90	$10^{-8.0}$	7.30	0.3	fsh
c72	J141741.9+522823	$817.2^{+29.6}_{-28.6}$	$544.7^{+24.4}_{-23.3}$	$274.5^{+17.6}_{-16.6}$	$72.5^{+9.6}_{-8.5}$	$50.00^{+1.80}_{-1.80}$	$13.00^{+0.59}_{-0.56}$	$38.00^{+2.40}_{-2.30}$	$20.00^{+2.60}_{-2.30}$	$10^{-8.0}$	0.20	−0.3	fshu
c73	J141742.8+522235	$3.7^{+3.6}_{-2.4}$	$4.9^{+3.6}_{-2.4}$	< 6.40	< 4.91	$0.63^{+0.38}_{-0.25}$	$0.34^{+0.20}_{-0.13}$	< 2.30	< 3.60	$10^{-5.7}$	5.80	−1.0	s
c74	J141743.2+522023	$14.3^{+5.7}_{-4.5}$	$12.1^{+5.0}_{-3.8}$	< 8.45	< 6.50	$2.20^{+0.58}_{-0.46}$	$0.69^{+0.23}_{-0.18}$	< 2.60	< 4.20	$10^{-6.9}$	8.00	−1.0	sf
c75	J141745.4+522951	$52.2^{+8.3}_{-7.2}$	$7.7^{+4.0}_{-2.8}$	$45.4^{+7.8}_{-6.8}$	$18.5^{+5.4}_{-4.3}$	$3.20^{+0.51}_{-0.44}$	$0.19^{+0.09}_{-0.06}$	$6.30^{+1.10}_{-0.93}$	$5.10^{+1.50}_{-1.20}$	$10^{-8.0}$	1.50	0.7	fshu
c76	J141745.7+522801	$54.6^{+8.5}_{-7.4}$	$37.8^{+7.2}_{-6.1}$	$17.6^{+5.3}_{-4.2}$	$7.7^{+4.0}_{-2.8}$	$6.10^{+0.94}_{-0.82}$	$1.70^{+0.31}_{-0.27}$	$4.40^{+1.30}_{-1.00}$	$3.80^{+1.90}_{-1.30}$	$10^{-8.0}$	0.60	−0.3	fshu
c77	J141745.9+523032	$239.2^{+16.5}_{-15.5}$	$121.7^{+12.1}_{-11.0}$	$119.4^{+12.0}_{-10.9}$	$38.4^{+7.3}_{-6.2}$	$15.00^{+1.00}_{-0.96}$	$3.00^{+0.29}_{-0.27}$	$17.00^{+1.70}_{-1.50}$	$10.00^{+2.00}_{-1.70}$	$10^{-8.0}$	2.20	0.0	fshu
c78	J141746.1+522526	$10.9^{+4.6}_{-3.4}$	$3.4^{+3.2}_{-1.9}$	$7.1^{+4.0}_{-2.8}$	< 4.32	$0.68^{+0.26}_{-0.19}$	$0.08^{+0.07}_{-0.04}$	$0.99^{+0.49}_{-0.34}$	< 1.10	$10^{-6.4}$	3.00	0.4	f
c79	J141746.7+522858	$12.3^{+4.7}_{-3.5}$	$8.7^{+4.1}_{-2.9}$	$3.4^{+3.2}_{-1.9}$	< 4.46	$0.76^{+0.28}_{-0.21}$	$0.21^{+0.10}_{-0.07}$	$0.47^{+0.38}_{-0.23}$	< 1.20	$10^{-8.0}$	0.80	−0.4	fs
c80	J141747.0+522512	$9.5^{+4.4}_{-3.3}$	< 4.28	$6.9^{+4.0}_{-2.8}$	< 5.14	$0.60^{+0.24}_{-0.18}$	< 0.11	$0.96^{+0.48}_{-0.33}$	< 1.30	$10^{-7.2}$	3.30	1.0	hf
c81	J141747.0+522816	$11.6^{+4.6}_{-3.4}$	$8.8^{+4.1}_{-2.9}$	$5.7^{+3.6}_{-2.4}$	< 3.73	$1.40^{+0.55}_{-0.41}$	$0.43^{+0.20}_{-0.14}$	$1.60^{+0.96}_{-0.63}$	< 2.00	$10^{-8.0}$	0.60	−0.2	fsh
c82	J141747.4+523510	$87.0^{+10.9}_{-9.8}$	$68.3^{+9.6}_{-8.5}$	$26.5^{+6.8}_{-5.7}$	< 7.87	$5.80^{+0.65}_{-0.59}$	$1.80^{+0.24}_{-0.21}$	$4.00^{+0.82}_{-0.69}$	< 2.30	$10^{-8.0}$	6.80	−0.4	fsh
c83	J141749.2+522803	$10.6^{+4.4}_{-3.3}$	$3.8^{+3.2}_{-1.9}$	$6.7^{+3.8}_{-2.6}$	< 3.71	$1.10^{+0.45}_{-0.33}$	$0.16^{+0.13}_{-0.08}$	$1.60^{+0.85}_{-0.58}$	< 1.60	$10^{-8.0}$	1.00	0.3	fh
c84	J141749.2+522811	$58.7^{+8.7}_{-7.7}$	$35.9^{+7.1}_{-6.0}$	$22.8^{+5.9}_{-4.8}$	$3.8^{+3.2}_{-1.9}$	$9.00^{+1.30}_{-1.20}$	$2.20^{+0.42}_{-0.36}$	$7.90^{+2.00}_{-1.60}$	$2.60^{+2.10}_{-1.20}$	$10^{-8.0}$	1.00	−0.2	fsh
c85	J141749.7+523143	$48.5^{+8.1}_{-7.0}$	$26.3^{+6.3}_{-5.2}$	$22.9^{+6.0}_{-4.9}$	$11.1^{+4.6}_{-3.4}$	$3.10^{+0.50}_{-0.43}$	$0.65^{+0.15}_{-0.13}$	$3.30^{+0.81}_{-0.66}$	$3.20^{+1.20}_{-0.90}$	$10^{-8.0}$	3.50	−0.1	fshu
c86	J141750.1+523601	$39.3^{+8.3}_{-7.2}$	$30.0^{+7.1}_{-6.0}$	$11.4^{+5.7}_{-4.5}$	< 10.02	$2.80^{+0.43}_{-0.38}$	$0.82^{+0.16}_{-0.14}$	$1.80^{+0.48}_{-0.38}$	< 3.10	$10^{-8.0}$	7.70	−0.4	fs
c87	J141750.5+522339	$25.2^{+6.4}_{-5.3}$	$10.6^{+4.6}_{-3.4}$	$15.1^{+5.2}_{-4.1}$	$3.7^{+3.4}_{-2.2}$	$2.10^{+0.48}_{-0.39}$	$0.35^{+0.13}_{-0.10}$	$2.80^{+0.85}_{-0.67}$	$1.30^{+0.90}_{-0.57}$	$10^{-8.0}$	4.90	0.2	fsh
c88	J141750.8+523632	$23.1^{+7.3}_{-6.2}$	$16.5^{+5.9}_{-4.8}$	< 11.80	< 9.98	$1.70^{+0.31}_{-0.27}$	$0.48^{+0.12}_{-0.10}$	< 1.80	< 3.20	$10^{-8.0}$	8.20	−1.0	fs
c89	J141751.0+522534	$24.0^{+6.1}_{-5.0}$	< 4.50	$23.2^{+6.0}_{-4.9}$	$12.4^{+4.7}_{-3.5}$	$1.70^{+0.41}_{-0.33}$	< 0.12	$3.60^{+0.90}_{-0.73}$	$3.70^{+1.40}_{-1.00}$	$10^{-8.0}$	3.10	1.0	fhu
c90	J141751.1+522310	$127.1^{+12.5}_{-11.4}$	$85.1^{+10.4}_{-9.3}$	$43.4^{+7.8}_{-6.8}$	$15.2^{+5.2}_{-4.1}$	$9.90^{+0.94}_{-0.86}$	$2.60^{+0.31}_{-0.28}$	$7.50^{+1.30}_{-1.10}$	$5.20^{+1.60}_{-1.30}$	$10^{-8.0}$	5.40	−0.3	fshu
c91	J141751.7+523046	$16.1^{+5.2}_{-4.1}$	$11.6^{+4.6}_{-3.4}$	$4.2^{+3.4}_{-2.2}$	< 4.37	$1.10^{+0.33}_{-0.26}$	$0.30^{+0.11}_{-0.09}$	$0.63^{+0.43}_{-0.27}$	< 1.20	$10^{-8.0}$	2.70	−0.4	fs
c92	J141752.4+522853	$26.3^{+6.3}_{-5.2}$	< 3.70	$24.4^{+6.1}_{-5.0}$	$8.5^{+4.1}_{-2.9}$	$1.70^{+0.40}_{-0.33}$	< 0.09	$3.60^{+0.88}_{-0.71}$	$2.50^{+1.10}_{-0.81}$	$10^{-8.0}$	1.50	1.0	fhu
c93	J141752.9+522838	$6.3^{+3.8}_{-2.6}$	< 3.70	< 4.45	< 4.50	$0.42^{+0.23}_{-0.15}$	< 0.10	< 0.63	< 1.30	$10^{-6.0}$	1.50	...	f
c94	J141753.1+522050	$21.0^{+6.9}_{-5.8}$	$10.8^{+5.2}_{-4.1}$	$10.4^{+5.4}_{-4.3}$	$3.7^{+4.1}_{-2.9}$	$1.60^{+0.32}_{-0.27}$	$0.32^{+0.10}_{-0.08}$	$1.80^{+0.50}_{-0.40}$	$1.30^{+0.59}_{-0.42}$	$10^{-7.2}$	7.70	0.0	f

Table 3 – *continued*

Cat. No. (1)	CXO GWS (2000) (2)	FB counts (3)	SB counts (4)	HB counts (5)	UB counts (6)	0.5–10.0 flux (7)	0.5–2.0 flux (8)	2–10 flux (9)	5–10 flux (10)	$p_{\rm min}$ (11)	OAA (arcmin) (12)	HR (13)	Flags (14)
c95	J141753.7+523446	$53.7^{+9.0}_{-7.9}$	< 9.07	$47.2^{+8.3}_{-7.2}$	$24.6^{+6.4}_{-5.3}$	$3.60^{+0.51}_{-0.45}$	< 0.24	$7.00^{+1.10}_{-0.96}$	$7.50^{+1.70}_{-1.40}$	$10^{-8.0}$	6.60	1.0	fhu
c96	J141753.9+523033	$17.1^{+5.3}_{-4.2}$	$10.6^{+4.4}_{-3.3}$	$6.3^{+3.8}_{-2.6}$	< 4.35	$1.10^{+0.32}_{-0.25}$	$0.26^{+0.11}_{-0.08}$	$0.89^{+0.48}_{-0.33}$	< 1.10	$10^{-8.0}$	2.70	−0.2	fsh
c97	J141754.2+523123	$50.6^{+8.3}_{-7.2}$	$40.4^{+7.5}_{-6.4}$	$11.9^{+4.7}_{-3.5}$	< 5.08	$3.20^{+0.51}_{-0.44}$	$1.00^{+0.18}_{-0.16}$	$1.70^{+0.61}_{-0.46}$	< 1.40	$10^{-8.0}$	3.40	−0.5	fsh
c98	J141754.5+523437	$15.2^{+6.0}_{-4.9}$	< 8.36	$15.4^{+5.7}_{-4.5}$	< 3.96	$1.00^{+0.25}_{-0.20}$	< 0.22	$2.30^{+0.62}_{-0.50}$	< 0.72	$10^{-8.0}$	6.50	1.0	hf
c99	J141755.2+523532	$40.3^{+8.3}_{-7.2}$	$29.5^{+7.1}_{-6.0}$	$15.9^{+6.0}_{-4.9}$	< 8.33	$2.70^{+0.43}_{-0.37}$	$0.79^{+0.15}_{-0.13}$	$2.40^{+0.60}_{-0.49}$	< 2.50	$10^{-8.0}$	7.40	−0.3	fsh
c100	J141756.7+522400	$38.7^{+7.5}_{-6.4}$	$25.4^{+6.3}_{-5.2}$	$14.8^{+5.2}_{-4.1}$	< 5.45	$2.60^{+0.47}_{-0.40}$	$0.68^{+0.16}_{-0.13}$	$2.20^{+0.69}_{-0.54}$	< 1.50	$10^{-8.0}$	4.90	−0.2	fsh
c101	J141756.8+523124	$72.2^{+9.6}_{-8.6}$	$45.2^{+7.8}_{-6.8}$	$27.8^{+6.4}_{-5.3}$	$9.0^{+4.3}_{-3.1}$	$4.60^{+0.60}_{-0.54}$	$1.10^{+0.19}_{-0.17}$	$4.00^{+0.88}_{-0.73}$	$2.60^{+1.10}_{-0.79}$	$10^{-8.0}$	3.70	−0.2	fshu
c102	J141756.9+523118	$5.3^{+3.8}_{-2.6}$	$4.2^{+3.4}_{-2.2}$	< 5.76	< 4.99	$0.34^{+0.18}_{-0.13}$	$0.11^{+0.07}_{-0.04}$	< 0.78	< 1.30	$10^{-5.4}$	3.60	−1.0	f
c103	J141757.1+522630	$100.0^{+11.1}_{-10.0}$	$46.5^{+7.9}_{-6.8}$	$59.1^{+8.8}_{-7.7}$	$15.3^{+5.1}_{-4.0}$	$6.30^{+0.69}_{-0.62}$	$1.10^{+0.19}_{-0.17}$	$8.20^{+1.20}_{-1.10}$	$4.10^{+1.30}_{-1.00}$	$10^{-8.0}$	2.90	0.1	fshu
c104	J141757.4+523106	$29.4^{+6.6}_{-5.5}$	$16.2^{+5.2}_{-4.1}$	$12.7^{+4.8}_{-3.7}$	$8.1^{+4.1}_{-2.9}$	$1.90^{+0.40}_{-0.34}$	$0.41^{+0.12}_{-0.10}$	$1.80^{+0.63}_{-0.48}$	$2.30^{+1.00}_{-0.74}$	$10^{-8.0}$	3.50	−0.1	fshu
c105	J141757.5+522546	$44.5^{+7.8}_{-6.8}$	$28.2^{+6.4}_{-5.3}$	$16.9^{+5.3}_{-4.2}$	< 4.21	$2.80^{+0.48}_{-0.41}$	$0.70^{+0.16}_{-0.13}$	$2.40^{+0.70}_{-0.55}$	< 1.10	$10^{-8.0}$	3.40	−0.2	fsh
c106	J141758.1+523133	$9.9^{+4.6}_{-3.4}$	$7.1^{+4.0}_{-2.8}$	< 5.56	< 4.95	$0.63^{+0.24}_{-0.18}$	$0.18^{+0.09}_{-0.06}$	< 0.75	< 1.30	$10^{-7.2}$	3.90	−1.0	f
c107	J141758.2+522153	$54.3^{+9.1}_{-8.0}$	$36.4^{+7.5}_{-6.4}$	$20.5^{+6.3}_{-5.2}$	< 8.74	$3.90^{+0.55}_{-0.48}$	$1.00^{+0.18}_{-0.16}$	$3.30^{+0.76}_{-0.63}$	< 2.70	$10^{-8.0}$	6.90	−0.3	fsh
c108	J141758.9+523138	$137.9^{+12.9}_{-11.8}$	$84.0^{+10.3}_{-9.2}$	$53.5^{+8.5}_{-7.4}$	$13.9^{+5.0}_{-3.8}$	$8.90^{+0.82}_{-0.75}$	$2.10^{+0.26}_{-0.23}$	$7.70^{+1.20}_{-1.00}$	$4.00^{+1.30}_{-1.00}$	$10^{-8.0}$	4.00	−0.2	fshu
c109	J141759.3+522420	$19.8^{+5.9}_{-4.8}$	$16.5^{+5.3}_{-4.2}$	$3.8^{+3.6}_{-2.4}$	< 5.57	$1.30^{+0.33}_{-0.26}$	$0.42^{+0.12}_{-0.10}$	$0.55^{+0.33}_{-0.22}$	< 1.50	$10^{-8.0}$	4.80	−0.6	fs
c110	J141800.0+522223	$162.1^{+14.1}_{-13.1}$	$80.0^{+10.2}_{-9.1}$	$86.8^{+10.7}_{-9.6}$	$30.2^{+6.9}_{-5.8}$	$11.00^{+0.90}_{-0.83}$	$2.10^{+0.26}_{-0.23}$	$13.00^{+1.50}_{-1.30}$	$9.20^{+1.90}_{-1.60}$	$10^{-8.0}$	6.60	0.1	fshu
c111	J141800.4+522822	$9.5^{+4.3}_{-3.1}$	< 2.94	$7.6^{+4.0}_{-2.8}$	< 3.69	$1.30^{+0.56}_{-0.40}$	< 0.15	$2.40^{+1.20}_{-0.82}$	< 2.20	$10^{-8.0}$	2.60	0.5	fh
c112	J141800.4+523610	$64.2^{+10.0}_{-9.0}$	$49.3^{+8.7}_{-7.6}$	$14.9^{+6.2}_{-5.1}$	$5.1^{+4.6}_{-3.4}$	$4.40^{+0.55}_{-0.49}$	$1.30^{+0.20}_{-0.18}$	$2.30^{+0.55}_{-0.45}$	$1.60^{+0.63}_{-0.47}$	$10^{-8.0}$	8.20	−0.5	fsh
c113	J141801.1+522941	$18.9^{+5.6}_{-4.4}$	$17.4^{+5.3}_{-4.2}$	< 5.07	< 4.28	$1.20^{+0.34}_{-0.27}$	$0.44^{+0.13}_{-0.10}$	< 0.69	< 1.20	$10^{-8.0}$	3.00	−1.0	fs
c114	J141801.3+523150	$11.5^{+4.8}_{-3.7}$	< 5.76	$9.1^{+4.4}_{-3.3}$	< 5.76	$0.74^{+0.26}_{-0.20}$	< 0.15	$1.30^{+0.53}_{-0.39}$	< 1.60	$10^{-8.0}$	4.40	1.0	fh
c115	J141801.6+522800	$11.9^{+4.7}_{-3.5}$	$8.4^{+4.1}_{-2.9}$	< 5.09	< 4.31	$0.75^{+0.27}_{-0.20}$	$0.21^{+0.10}_{-0.07}$	< 0.68	< 1.20	$10^{-8.0}$	2.90	−1.0	fs
c116	J141802.0+523514	$324.3^{+19.4}_{-18.4}$	$253.5^{+17.1}_{-16.1}$	$80.5^{+10.5}_{-9.4}$	$24.8^{+6.6}_{-5.4}$	$22.00^{+1.30}_{-1.20}$	$6.90^{+0.45}_{-0.43}$	$12.00^{+1.50}_{-1.30}$	$7.90^{+1.70}_{-1.40}$	$10^{-8.0}$	7.40	−0.5	fshu
c117	J141802.4+522132	$53.5^{+9.2}_{-8.1}$	$40.6^{+7.9}_{-6.8}$	$14.9^{+5.9}_{-4.8}$	$5.9^{+4.4}_{-3.3}$	$3.70^{+0.51}_{-0.45}$	$1.10^{+0.18}_{-0.16}$	$2.30^{+0.59}_{-0.47}$	$1.90^{+0.75}_{-0.55}$	$10^{-8.0}$	7.50	−0.4	fsh
c118	J141802.9+523547	$100.1^{+11.8}_{-10.7}$	$71.3^{+9.9}_{-8.9}$	$29.6^{+7.3}_{-6.2}$	$9.3^{+5.0}_{-3.8}$	$7.50^{+0.76}_{-0.69}$	$2.10^{+0.26}_{-0.24}$	$4.90^{+0.92}_{-0.78}$	$3.20^{+1.10}_{-0.82}$	$10^{-8.0}$	8.00	−0.4	fshu
c119	J141804.5+523633	$150.5^{+14.0}_{-13.0}$	$119.8^{+12.4}_{-11.3}$	$42.0^{+8.4}_{-7.3}$	$10.9^{+5.3}_{-4.2}$	$12.00^{+1.00}_{-0.92}$	$3.80^{+0.36}_{-0.33}$	$7.50^{+1.20}_{-1.00}$	$4.10^{+1.20}_{-0.96}$	$10^{-8.0}$	8.80	−0.5	fshu
c120	J141804.8+522740	$44.4^{+7.8}_{-6.8}$	$31.2^{+6.7}_{-5.6}$	$13.8^{+5.0}_{-3.8}$	< 5.07	$2.90^{+0.50}_{-0.43}$	$0.81^{+0.17}_{-0.14}$	$2.00^{+0.67}_{-0.52}$	< 1.40	$10^{-8.0}$	3.40	−0.4	fsh
c121	J141805.3+522510	$38.0^{+7.5}_{-6.4}$	$24.6^{+6.2}_{-5.1}$	$13.9^{+5.1}_{-4.0}$	< 5.62	$2.60^{+0.48}_{-0.41}$	$0.67^{+0.16}_{-0.13}$	$2.10^{+0.68}_{-0.53}$	< 1.60	$10^{-8.0}$	4.70	−0.3	fsh
c122	J141806.5+523358	$19.4^{+6.3}_{-5.2}$	$11.6^{+5.0}_{-3.8}$	$6.9^{+4.6}_{-3.4}$	< 7.79	$1.40^{+0.33}_{-0.27}$	$0.34^{+0.11}_{-0.09}$	$1.10^{+0.43}_{-0.32}$	< 2.50	$10^{-8.0}$	6.60	−0.2	fs
c123	J141807.0+522523	$102.6^{+11.3}_{-10.3}$	$59.3^{+8.9}_{-7.8}$	$44.8^{+7.9}_{-6.8}$	$11.4^{+4.7}_{-3.5}$	$6.60^{+0.71}_{-0.65}$	$1.50^{+0.22}_{-0.19}$	$6.50^{+1.10}_{-0.94}$	$3.20^{+1.20}_{-0.89}$	$10^{-8.0}$	4.70	−0.1	fsh
c124	J141807.3+523030	$4.9^{+3.8}_{-2.6}$	$4.1^{+3.4}_{-2.2}$	< 5.40	< 5.81	$0.37^{+0.20}_{-0.13}$	$0.12^{+0.08}_{-0.05}$	< 0.85	< 1.90	$10^{-5.6}$	4.20	−1.0	s
c125	J141808.0+522750	$11.9^{+4.8}_{-3.7}$	$5.9^{+3.8}_{-2.6}$	$6.5^{+4.0}_{-2.8}$	$6.0^{+3.8}_{-2.6}$	$0.79^{+0.27}_{-0.21}$	$0.15^{+0.08}_{-0.06}$	$0.97^{+0.48}_{-0.34}$	$1.80^{+0.97}_{-0.66}$	$10^{-6.6}$	3.90	0.1	f
c126	J141808.9+523150	$10.0^{+4.8}_{-3.7}$	< 6.14	$8.1^{+4.4}_{-3.3}$	$7.0^{+4.1}_{-2.9}$	$0.66^{+0.23}_{-0.17}$	< 0.16	$1.20^{+0.48}_{-0.35}$	$2.00^{+0.94}_{-0.67}$	$10^{-6.4}$	5.20	1.0	f

Table 3 – *continued*

Cat. No. (1)	CXO GWS (2000) (2)	FB counts (3)	SB counts (4)	HB counts (5)	UB counts (6)	0.5–10.0 flux (7)	0.5–2.0 flux (8)	2–10 flux (9)	5–10 flux (10)	$p_{\min}$ (11)	OAA (arcmin) (12)	HR (13)	Flags (14)
c127	J141809.1+522804	$49.7^{+8.3}_{-7.2}$	$24.9^{+6.2}_{-5.1}$	$24.4^{+6.2}_{-5.1}$	$10.0^{+4.4}_{-3.3}$	$3.50^{+0.56}_{-0.49}$	$0.70^{+0.17}_{-0.14}$	$4.00^{+0.94}_{-0.77}$	$3.30^{+1.30}_{-0.97}$	$10^{-8.0}$	4.00	0.0	fshu
c128	J141811.2+523011	$15.6^{+5.4}_{-4.3}$	$9.6^{+4.4}_{-3.3}$	$6.6^{+4.1}_{-2.9}$	< 6.33	$1.00^{+0.29}_{-0.23}$	$0.25^{+0.10}_{-0.07}$	$0.97^{+0.44}_{-0.32}$	< 1.80	$10^{-8.0}$	4.60	−0.2	fs
c129	J141812.1+522800	$29.3^{+6.8}_{-5.7}$	$20.3^{+5.8}_{-4.7}$	$9.6^{+4.6}_{-3.4}$	< 5.46	$1.90^{+0.39}_{-0.33}$	$0.52^{+0.14}_{-0.11}$	$1.40^{+0.54}_{-0.40}$	< 1.50	$10^{-8.0}$	4.40	−0.3	fs
c130	J141813.1+523113	$50.4^{+8.5}_{-7.4}$	$34.9^{+7.1}_{-6.1}$	$17.9^{+5.7}_{-4.5}$	$8.8^{+4.4}_{-3.3}$	$3.30^{+0.51}_{-0.45}$	$0.91^{+0.18}_{-0.15}$	$2.60^{+0.71}_{-0.57}$	$2.60^{+1.10}_{-0.78}$	$10^{-8.0}$	5.40	−0.3	fsh
c131	J141813.3+522414	$18.6^{+6.1}_{-5.0}$	$12.8^{+5.1}_{-4.0}$	< 8.60	< 7.27	$1.50^{+0.37}_{-0.30}$	$0.41^{+0.13}_{-0.10}$	< 1.50	< 2.50	$10^{-8.0}$	6.20	−1.0	fs
c132	J141813.9+522624	$17.5^{+5.8}_{-4.7}$	$3.6^{+3.6}_{-2.4}$	$13.1^{+5.1}_{-4.0}$	< 6.12	$1.10^{+0.30}_{-0.24}$	$0.09^{+0.06}_{-0.04}$	$1.90^{+0.61}_{-0.47}$	< 1.70	$10^{-8.0}$	5.10	0.6	fh
c133	J141814.2+522810	$24.0^{+6.4}_{-5.3}$	$24.1^{+6.2}_{-5.1}$	$5.3^{+4.0}_{-2.8}$	< 6.19	$1.60^{+0.35}_{-0.29}$	$0.62^{+0.15}_{-0.12}$	$0.78^{+0.39}_{-0.27}$	< 1.80	$10^{-8.0}$	4.80	−0.6	fs
c134	J141815.3+523247	$43.3^{+8.3}_{-7.2}$	$31.3^{+7.0}_{-5.9}$	$11.8^{+5.3}_{-4.2}$	< 7.96	$2.90^{+0.47}_{-0.40}$	$0.83^{+0.17}_{-0.14}$	$1.80^{+0.52}_{-0.41}$	< 2.30	$10^{-8.0}$	6.60	−0.4	fs
c135	J141816.2+522940	$369.2^{+20.4}_{-19.3}$	$287.0^{+18.0}_{-17.0}$	$86.6^{+10.5}_{-9.5}$	$19.7^{+5.8}_{-4.7}$	$25.00^{+1.30}_{-1.30}$	$7.50^{+0.47}_{-0.44}$	$13.00^{+1.50}_{-1.40}$	$6.00^{+1.60}_{-1.30}$	$10^{-8.0}$	5.20	−0.5	fshu
c136	J141816.3+522524	$59.5^{+9.2}_{-8.1}$	$41.7^{+7.8}_{-6.7}$	$19.5^{+6.0}_{-4.9}$	< 7.17	$4.00^{+0.55}_{-0.49}$	$1.10^{+0.19}_{-0.16}$	$2.90^{+0.72}_{-0.59}$	< 2.00	$10^{-8.0}$	5.90	−0.3	fsh
c137	J141816.4+523329	$26.6^{+7.2}_{-6.1}$	$14.7^{+5.6}_{-4.4}$	$11.1^{+5.4}_{-4.3}$	< 8.91	$1.80^{+0.35}_{-0.29}$	$0.40^{+0.11}_{-0.09}$	$1.70^{+0.48}_{-0.38}$	< 2.60	$10^{-8.0}$	7.20	−0.1	fs
c138	J141816.7+522307	$139.6^{+13.4}_{-12.4}$	$104.8^{+11.6}_{-10.5}$	$38.8^{+8.0}_{-6.9}$	< 9.45	$9.60^{+0.84}_{-0.77}$	$2.80^{+0.29}_{-0.27}$	$6.00^{+1.00}_{-0.86}$	< 2.80	$10^{-8.0}$	7.40	−0.4	fsh
c139	J141818.0+523201	$28.8^{+7.1}_{-6.1}$	$17.3^{+5.7}_{-4.5}$	$11.4^{+5.2}_{-4.1}$	< 7.49	$2.00^{+0.39}_{-0.33}$	$0.47^{+0.13}_{-0.10}$	$1.80^{+0.54}_{-0.42}$	< 2.30	$10^{-8.0}$	6.40	−0.2	fs
c140	J141819.9+522115	$25.0^{+8.0}_{-6.9}$	$8.6^{+5.6}_{-4.4}$	$15.1^{+6.6}_{-5.4}$	< 10.51	$1.90^{+0.32}_{-0.27}$	$0.26^{+0.07}_{-0.06}$	$2.60^{+0.57}_{-0.48}$	< 3.70	$10^{-6.6}$	9.10	0.3	f
c141	J141820.3+523351	$28.9^{+7.7}_{-6.6}$	$20.7^{+6.4}_{-5.3}$	< 11.96	< 9.96	$2.00^{+0.35}_{-0.30}$	$0.56^{+0.13}_{-0.11}$	< 1.80	< 3.00	$10^{-6.9}$	7.90	−1.0	fs
c142	J141821.3+522655	$21.9^{+6.4}_{-5.3}$	$14.4^{+5.3}_{-4.2}$	< 9.11	< 7.87	$1.50^{+0.34}_{-0.28}$	$0.40^{+0.12}_{-0.09}$	< 1.40	< 2.40	$10^{-8.0}$	6.00	−1.0	fs
c143	J141821.3+523254	$26.3^{+7.3}_{-6.2}$	$14.9^{+5.7}_{-4.5}$	$14.2^{+5.9}_{-4.8}$	< 4.57	$1.80^{+0.34}_{-0.29}$	$0.40^{+0.11}_{-0.09}$	$2.20^{+0.55}_{-0.45}$	< 0.76	$10^{-8.0}$	7.40	0.0	fsh
c144	J141821.7+522955	$20.6^{+6.4}_{-5.3}$	$21.5^{+6.1}_{-5.0}$	< 9.04	< 8.35	$1.40^{+0.31}_{-0.26}$	$0.58^{+0.14}_{-0.11}$	< 1.30	< 2.50	$10^{-8.0}$	6.10	−1.0	fs
c145	J141822.0+522650	$36.2^{+7.7}_{-6.6}$	$25.2^{+6.4}_{-5.3}$	$10.8^{+5.1}_{-4.0}$	$7.7^{+4.4}_{-3.3}$	$2.50^{+0.44}_{-0.38}$	$0.69^{+0.15}_{-0.13}$	$1.70^{+0.54}_{-0.42}$	$2.40^{+0.98}_{-0.72}$	$10^{-8.0}$	6.10	−0.4	fs
c146	J141822.4+523607	$163.6^{+15.1}_{-14.0}$	$110.7^{+12.3}_{-11.2}$	$58.5^{+10.0}_{-8.9}$	$18.9^{+6.6}_{-5.5}$	$12.00^{+0.90}_{-0.84}$	$3.10^{+0.30}_{-0.28}$	$9.50^{+1.20}_{-1.10}$	$6.50^{+1.40}_{-1.20}$	$10^{-8.0}$	9.80	−0.3	fshu
c147	J141822.8+522710	$22.1^{+6.6}_{-5.4}$	$22.0^{+6.2}_{-5.1}$	< 8.82	< 7.58	$1.60^{+0.34}_{-0.28}$	$0.61^{+0.14}_{-0.12}$	< 1.30	< 2.30	$10^{-8.0}$	6.20	−1.0	fs
c148	J141823.0+522114	$43.1^{+9.4}_{-8.3}$	$16.5^{+6.4}_{-5.3}$	$25.5^{+7.7}_{-6.6}$	< 11.93	$3.20^{+0.43}_{-0.39}$	$0.48^{+0.11}_{-0.09}$	$4.30^{+0.75}_{-0.65}$	< 4.10	$10^{-8.0}$	9.40	0.2	fh
c149	J141824.9+522330	$290.0^{+18.5}_{-17.5}$	$156.3^{+13.8}_{-12.8}$	$138.1^{+13.2}_{-12.2}$	$33.6^{+7.4}_{-6.3}$	$21.00^{+1.30}_{-1.20}$	$4.50^{+0.38}_{-0.35}$	$23.00^{+2.00}_{-1.90}$	$12.00^{+2.10}_{-1.80}$	$10^{-8.0}$	8.10	0.0	fshu
c150	J141825.5+522349	$193.6^{+15.5}_{-14.4}$	$140.7^{+13.2}_{-12.1}$	$55.8^{+9.2}_{-8.1}$	$19.8^{+6.2}_{-5.1}$	$14.00^{+1.00}_{-0.97}$	$4.00^{+0.36}_{-0.33}$	$9.10^{+1.30}_{-1.10}$	$6.80^{+1.60}_{-1.30}$	$10^{-8.0}$	7.90	−0.4	fshu
c151	J141826.3+522818	$98.1^{+11.5}_{-10.4}$	$89.6^{+10.8}_{-9.7}$	$22.6^{+6.6}_{-5.4}$	< 9.18	$6.60^{+0.70}_{-0.64}$	$2.40^{+0.27}_{-0.24}$	$3.50^{+0.77}_{-0.64}$	< 2.80	$10^{-8.0}$	6.60	−0.6	fsh
c152	J141826.4+523235	$17.7^{+6.9}_{-5.8}$	$19.8^{+6.3}_{-5.2}$	< 12.67	< 10.21	$1.20^{+0.25}_{-0.21}$	$0.54^{+0.13}_{-0.10}$	< 1.90	< 3.10	$10^{-8.0}$	7.80	−1.0	sf
c153	J141826.5+522559	$31.2^{+7.5}_{-6.4}$	$11.7^{+5.2}_{-4.1}$	$19.7^{+6.3}_{-5.2}$	< 8.55	$2.20^{+0.40}_{-0.34}$	$0.33^{+0.10}_{-0.08}$	$3.20^{+0.73}_{-0.60}$	< 2.70	$10^{-8.0}$	7.00	0.3	fsh
c154	J141829.7+522709	$27.2^{+7.4}_{-6.3}$	$10.8^{+5.2}_{-4.1}$	$18.4^{+6.3}_{-5.2}$	$8.7^{+4.8}_{-3.7}$	$2.00^{+0.36}_{-0.31}$	$0.30^{+0.09}_{-0.07}$	$3.00^{+0.69}_{-0.57}$	$2.90^{+1.00}_{-0.76}$	$10^{-8.0}$	7.20	0.3	fh
c155	J141830.2+522212	$1118.2^{+34.9}_{-33.9}$	$885.5^{+31.0}_{-30.0}$	$265.4^{+17.9}_{-16.9}$	$68.5^{+10.0}_{-8.9}$	$81.00^{+2.40}_{-2.40}$	$25.00^{+0.86}_{-0.83}$	$44.00^{+2.70}_{-2.60}$	$24.00^{+3.00}_{-2.70}$	$10^{-8.0}$	9.50	−0.5	fshu
c156	J141832.8+522349	$83.4^{+11.4}_{-10.3}$	$61.9^{+9.6}_{-8.6}$	$23.8^{+7.3}_{-6.2}$	$10.5^{+5.4}_{-4.3}$	$6.40^{+0.68}_{-0.62}$	$1.90^{+0.24}_{-0.22}$	$4.10^{+0.78}_{-0.66}$	$3.80^{+1.10}_{-0.88}$	$10^{-8.0}$	8.90	−0.4	fsh
c157	J141837.9+522034	$25.8^{+9.8}_{-8.8}$	$19.2^{+7.4}_{-6.3}$	< 8.55	< 14.74	$2.40^{+0.31}_{-0.27}$	$0.72^{+0.13}_{-0.11}$	< 1.70	< 6.70	$10^{-5.6}$	11.50	−1.0	s
c158	J141838.1+522358	$129.2^{+12.8}_{-11.7}$	$99.3^{+11.2}_{-10.2}$	$32.6^{+7.2}_{-6.1}$	< 7.05	$39.00^{+3.60}_{-3.30}$	$11.00^{+1.20}_{-1.10}$	$22.00^{+4.20}_{-3.60}$	< 9.70	$10^{-8.0}$	9.50	−0.5	fsh

in the detection run, where $N_{\rm pix}$ is the total number of pixels in the image. The ACIS-I image of the GWS has a total of 4.41×10^6 pixels, so according to this prescription ∼0.44 spurious sources are expected in each of the four images and 1.8 in all four. The total number of detected sources was 134 (FB), 114 (SB), 86 (HB) and 41 (UB). This compares to 155, 121, 100, 44 using our method (Table 2). Thus, our method produces more sources than WAVDETECT at the probability threshold level that is generally used for ACIS-I images, when we use a threshold expected to match WAVDETECT in terms of false sources.

Matching the catalogues shows that only two sources are detected in the WAVDETECT run that are not identified in our procedure. Conversely 19 additional sources are detected with our method that are not found by WAVDETECT. We have visually inspected all of these sources and are confident of their reality. Sometimes these new sources are at the edge of the chips (e.g. c2), or in the chip gaps (c68, c69). In one case (c52, c53) we find two sources very close together, while WAVDETECT identifies only one as significant. Some caution needs to be applied in this case.

We also investigated the effect of a lower $p_{\rm thresh}$ values by repeating the WAVDETECT detection at $p_{\rm thresh} = 10^{-6}$, 10^{-5} and 10^{-4}. The results are shown in Table 2. It can be seen that at a probability of 10^{-6} WAVDETECT becomes more sensitive than our method, but with an unacceptably high fraction (>10 per cent) of spurious sources. Interestingly, the expected number of spurious sources at the 10^{-4} probability level exceeds the total number of detections at that level (1384). As many of the latter are actually real sources, there is some evidence that the WAVDETECT rule of thumb overestimates the number of false sources. If so, WAVDETECT could be run at probability levels lower then 10^{-7} without fear of excessive false detections, revealing the additional objects found in our analysis. The key point we make here, however, is that the additional sources we detect are very probably real, but would have been missed had we blindly used the typical WAVDETECT threshold of 10^{-7}.

4.1.2 Comparison fields

We have also performed source detection for two comparison fields, the *ISO* ELAIS-N1 field, for which *Chandra* data have been presented previously by Manners et al. (2003, hereafter M03), and the 2 Ms HDF-N (Alexander et al. 2003). Our standard screening procedure applied to ELAIS-N1 resulted in an exposure of 70 ks. The HDF-N analysis is described in more detail by Laird et al. (in preparation), and is more complicated than that described above, as there are multiple pointings with very different aim points and roll angles. Our detection procedure resulted in a total of 145 sources for ELAIS-N1, and 536 for the HDF-N applying a threshold probability of 4×10^{-6} as for the GWS. Again these compare favourably to WAVDETECT. M03 report 127 ACIS-I sources in ELAIS-N1 and A03 report 503 for HDF-N. The analysis of the comparison fields is discussed further in the Appendix.

4.2 X-ray number counts

We have calculated the detection sensitivity as a function of area for three of the bands (SB, HB, UB) according to the prescription described above. This is shown in Fig. 2. The limiting fluxes in each band, defined as the flux to which at least 1 per cent of the survey area is sensitive, are 1.1×10^{-16} (SB), 8.2×10^{-16} (HB) and 1.4×10^{-15} erg cm^{-2} s^{-1} (UB). The total survey area is 0.082 deg^{-2}. The limiting flux in the full band is 3.5×10^{-15} erg cm^{-2} s^{-1}, which can be compared to the limit of the *XMM* survey given by Waskett et al. (2004) of approximately 2×10^{-15} erg cm^{-2} s^{-1}, i.e. the deepest part of our *Chandra* survey probes fluxes about five or six times deeper than the *XMM* survey. Averaged over the whole field, we detect about three times as many sources per unit area as the *XMM* survey, but note that the *XMM* field is around three times larger than that of ACIS-I, so the total number of sources is very similar.

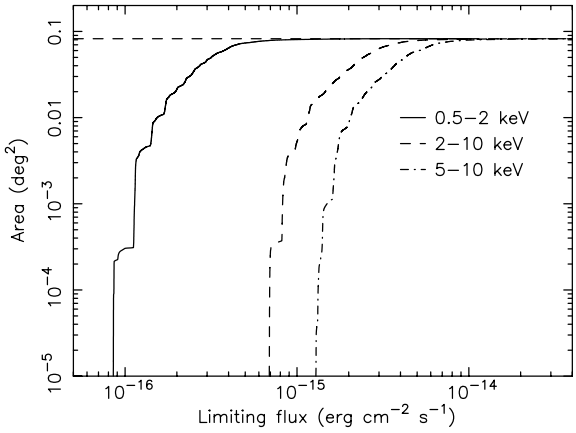

Figure 2. Limiting flux against survey area in the three bands for which we have calculated the $\log N - \log S$ function: SB (0.5–2 keV, solid line), HB (2–10 keV, dashed line), and UB (5–10 keV, dot-dashed line). The total survey area is 0.082 deg^2.

The cumulative number count distributions ($\log N - \log S$) for the GWS are shown in Fig. 3. For comparison, we also show the distributions from the ELAIS-N1 deep survey (M03) and the HDF-N (Brandt et al. 2001a; A03). The source density in the GWS is generally lower than in the other fields, which may indicate that we are sampling a relative void in the large-scale structure. 'Cosmic variance' of this kind has been suggested by previous investigations (e.g. Yang et al. 2003). For example, M03, comparing the ELAIS-N1 (analysed here) and ELAIS-N2 fields, report that the former has ∼30 per cent higher number counts, and attribute this to large-scale clustering. We can investigate this with our data also. For example, comparing the soft X-ray $\log N - \log S$ we can see that, at a representative flux level of 10^{-15}, above the level where incompleteness and Eddington bias should seriously affect the results, the ELAIS-N1 counts are ∼50 per cent higher than those in the GWS. When we consider the expected Poissonian errors, however, we find the source densities of 827 ± 100 and 570 ± 84 deg^{-2} are consistent at the 2σ level. The differences in number counts in the hard band are less significant than this.

4.3 Spectral properties

4.3.1 Hardness ratios

The hardness ratios of all objects in our sample are given in Table 3, and our relatively lax criterion for cross-band detection means that this quantity is defined for the great majority of sources. This allows us to calculate the mean hardness ratio for the entire sample, and also for objects detected in the various sub-bands. As discussed by Nandra et al. (2003), when attempting to characterize the mean spectrum of an X-ray survey sample it is preferable to adopt the unweighted average of the hardness ratio. This is because using the weighted average, or count stacking, can mean that the result is dominated by a few bright sources. This is particularly important

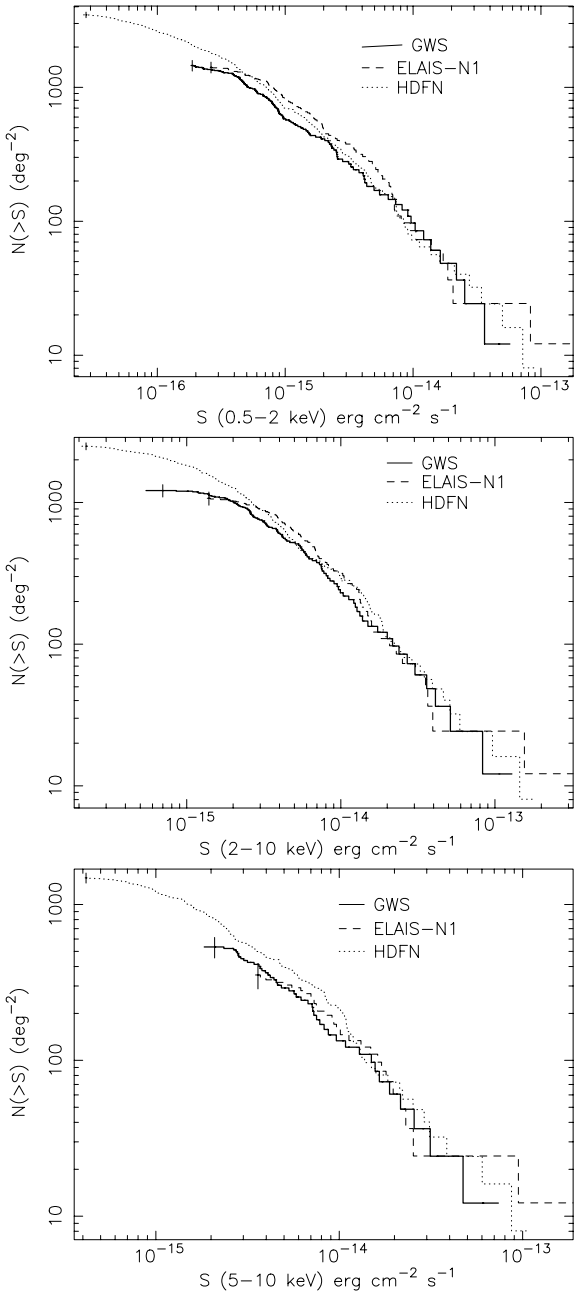

Figure 3. Cumulative $\log N - \log S$ functions for the SB, HB and UB for the Groth Strip and the two comparison fields (ELAIS-N1 and HDF-N). The faintest flux point for each field shows the Poisson error bar. The source counts in all three bands are generally lower in the GWS compared to the comparison fields, showing that it samples a relative void. However, even comparing to the field with the highest source density (ELAIS-N1), we find no significant evidence that the number counts differ beyond the expected Poisson variations (see text). The source counts show the effects of incompleteness at the faintest fluxes probed by each survey.

when it is suspected that the spectral properties might depend on flux, as has been suggested for *Chandra* samples (e.g. Giacconi et al. 2001). We find the following unweighted mean hardness ratio for sources detected in the various bands: -0.19 ± 0.05 (FB), -0.42 ± 0.03 (SB), -0.01 ± 0.05 (HB) and -0.06 ± 0.07 (UB). The hardness values in Table 3 have been calculated based on the counts corrected to on-axis values. They have not been corrected for the ACISABS effect, as we apply this when calculating the fluxes. We have considered this correction, however, when converting the hardness values to effective spectral indices, which we have performed using PIMMS. They are $\Gamma = 1.4 \pm 0.1$ (FB – note that the same value is found when considering the whole sample of 158 sources), $\Gamma = 1.85 \pm 0.05$ (SB), $\Gamma = 1.0 \pm 0.1$ (HB) and $\Gamma = 1.1 \pm 0.1$ (UB). There is clearly a highly significant difference in the mean spectrum of sources selected in the soft and hard bands ($\sim 7.5\sigma$).

4.3.2 *Spectral fitting*

In addition to hardness ratio analysis, we have also performed direct spectral fitting on our sources. Spectra were extracted using the CIAO tool PSEXTRACT for the detected sources, using the 95 per cent PSF region for the full band, and the background using an annular region as described for the source detection. We performed spectral fitting only on sources with >80 source plus background counts, to give at least four bins with a minimum of 20 counts per bin, permitting a χ^2 fitting procedure. A total of 56 sources satisfied this criterion. We performed the fits in XSPEC, starting with a simple power law with Galactic absorption ($N_{\rm H} = 1.27 \times 10^{20}$ cm^{-2}; Dickey & Lockman 1990). This proved a formally satisfactory fit in the great majority of cases, with only nine sources being inconsistent with this model at >99 per cent confidence. The photon index (Γ) is plotted against flux in Fig. 4.

The objects display a very wide range of photon indices, from $\Gamma = -0.5$ to 2.2. They are completely inconsistent with a single universal index, a hypothesis rejected at >99.99 per cent confidence. The unweighted average index, of $\Gamma = 1.29 \pm 0.08$, is very much consistent with that determined from the hardness ratio analysis, so while the spectral subsample tends to be brighter it is representative

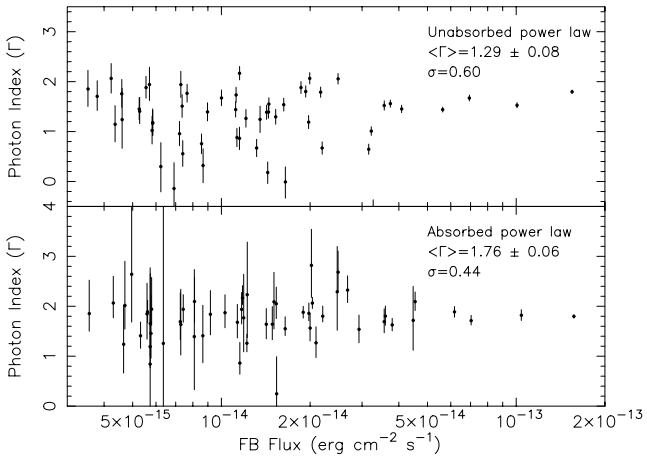

Figure 4. Power-law photon index versus full band flux for the 56 sources with >80 total counts (FB) in a region defined by the 95 per cent PSF. The upper panel shows the results with Galactic $N_{\rm H}$ only. A wide dispersion of photon indices is observed, the data being completely inconsistent with a constant (reduced $\chi^2 = 12.8$). The mean index (unweighted) is consistent with that derived from the hardness ratio analysis and shows that these sources are representative of the full sample, and of the objects that make up the XRB. When additional absorption is included (lower panel), the dispersion reduces substantially, with the objects now being consistent with a single index of $\Gamma \sim 1.8$, similar to local Seyferts (Nandra & Pounds 1994). Only a relatively small proportion of the objects require this additional absorption, however. Fluxes in the lower panel are corrected for intrinsic absorption. A single point with best-fitting $\Gamma \sim 7$ and very large error bars has been omitted for clarity.

of the sample as a whole. The weighted average index is $\Gamma = 1.51 \pm 0.02$, slightly softer than the X-ray background (XRB) but still consistent with the mean spectrum from the hardness ratio analysis.

Nine of the objects show a spectrum inconsistent at >99 per cent confidence with a single power law absorbed by the Galactic $N_{\rm H}$ based on their χ^2. The most likely reason for this, and the hardness of the spectra, is absorption. We have tested this by introducing a neutral absorber into the model. As we do not have redshifts for the majority of the objects at present, we fix the absorber at $z = 0$. This means that the derived column densities from the fits will not be accurate and we do not quote them. The fits should, however, give a reasonably accurate test of whether or not absorption is present in a given object, and of the effects of absorption on the power-law index. This is because the photoelectric cross-section in the soft X-rays is dominated by K-shell absorption by moderate-Z elements, which has an approximate E^{-3} form for a wide range of atomic number.

When absorption is allowed in the fit, a significant improvement (at >99 per cent confidence based on the *F*-test) is found in eight objects. A more marginal improvement seen in some others is none the less likely to indicate the presence of absorption – for example, c17 shows an acceptable fit when absorption is included, where it was previously unacceptable. Indeed, no source exhibits a spectrum inconsistent with this absorbed power-law model at >99 per cent confidence. More complex models are not therefore required, nor would they be particularly meaningful without the redshifts. In the absorbed model, the objects are now consistent with a universal index, of $\Gamma = 1.76 \pm 0.08$.

Absorption clearly has a very substantial effect on the mean spectral properties, but as in the hardness ratio analysis the number of objects with significant absorption appears small. Only ∼15 per cent of the spectral subsample (8/56) shows clear evidence for $N_{\rm H}$ above the Galactic value. Some of this may be due to poor spectral quality – the weakest source in which absorption is detected has ∼160 counts, and we may simply be insensitive to absorption in objects fainter than this. Even if we restrict the analysis to objects with more counts than this limit, however, we still find only 25 per cent of objects (8/32) with significant absorption.

5 DISCUSSION

We have presented a source catalogue, number counts and spectral properties for the 200-ks deep survey of the GWS performed by *Chandra*. There have been a large variety of methods applied in the literature to identify sources, assign significances, determine fluxes and errors, and determine limiting sensitivities. Finding none of these entirely satisfactory, we have developed our own procedure based on pre-identification of candidate sources with WAVDETECT, and a simple aperture extraction using the 70 per cent PSF and a local background to determine significances. This procedure is statistically well defined, and it finds more sources than WAVDETECT – arguably the most common source detection procedure used in the literature. A total of 158 independent sources are detected in our band-merged catalogue, with the great majority (>75 per cent) being detected in the soft band and no source being detected exclusively in the hard or ultra-hard bands.

Observations have suggested significant differences in the number counts from field to field, which have been attributed to 'cosmic variance' (e.g. Cowie et al. 2002; Yang et al. 2003), but one study (Kim et al. 2004) has reported no such effect. Clearly it is important to investigate this issue further with deep survey data, and we have done so with the GWS. While the $\log N - \log S$ function shows lower counts than our comparison fields (by ∼50 per cent compared to ELAIS-N1), we find the statistical significance of the difference in number counts to be weak ($<2\sigma$). This is not entirely surprising in that, at the fluxes where the $\log N - \log S$ is generally compared, the typical number of detected *Chandra* sources per *Chandra* field is very small (e.g. ∼25 at 10^{-14} erg cm^{-2} s^{-1} in the hard band). Large differences are therefore expected purely from Poisson variations. Greater source numbers – and hence lower Poisson noise – are present at fainter fluxes, but here the number counts appear to be consistent. As discussed by Yang et al., the main evidence for 'cosmic variance' from the number counts comes from only two fields (including the CDF-S), which show low source numbers and apparently sample a relative void and only in the hard band. It is clear also from the presence of 'spikes' in the redshift distribution of X-ray-selected sources (e.g. Barger et al. 2002; Gilli et al. 2003) in deep surveys that there must be significant field-to-field variations in the X-ray source population. We simply point out here that even large variations (∼50 per cent) in the number counts do not necessarily mean that there is significant cosmic variance, and we await further observations to confirm or deny the presence of these X-ray voids.

Perhaps the most interesting result from our current analysis comes from the spectra. The whole sample (essentially the FB sources) shows a mean spectrum of $\Gamma = 1.3$ –1.5 from both the hardness ratio and direct spectral analysis. This is consistent with that of the XRB, which is encouraging as our survey resolves the majority of that background. On the other hand, we find a very marked difference between the mean spectra of soft and hard X-ray-selected sources. The former have $\Gamma = 1.9$. This mean spectrum is also in agreement with the average spectrum of (brighter) *ROSAT*-selected AGN (Georgantopoulos et al. 1997; Blair et al. 2000). It is also typical of the intrinsic spectrum of local AGN (Nandra & Pounds 1994). The implication is that these soft X-ray sources suffer essentially no obscuration. On the other hand, the hard X-ray-selected (2–7 keV) sources show $\Gamma = 1.0$, significantly flatter than the XRB. Once again this shows good consistency with brighter hard X-ray-selected samples, e.g. the 5–10 keV selected SHEEP sample (Nandra et al. 2003). The surprise comes when we consider the fact that over 75 per cent of the whole sample is detected in the soft band, and hence relatively unobscured with mean $\Gamma = 1.9$. Only a very small (25 per cent) population of heavily obscured objects detected in the hard band are therefore required to flatten the XRB to its observed level.

Direct spectral fitting of our *Chandra* data confirms this result, which is also found in *XMM* samples, which probe slightly brighter fluxes (Piconcelli et al. 2003; Georgantopoulos et al. 2004). Our survey probes deeper into the populations producing the XRB and shows clearly and directly that the majority of objects producing that background are relatively unobscured in the X-ray. This is completely at odds with standard population synthesis models for the XRB (e.g. Comastri et al. 1995; Gilli, Risaliti & Salvati 1999; Gilli, Salvati & Hasinger 2001), which predict that obscured sources should dominate. The basis of these synthesis models is the Type I/II unification scheme, which has proved so successful in explaining the properties of local AGN (Antonucci & Miller 1985). Given the lack of correspondence between X-ray and optical measures of obscuration that is emerging in X-ray-selected objects (e.g. Pappa et al. 2001; Comastri et al. 2001; Nandra et al. 2004), the basis of these synthesis models is also in doubt and they need to be examined completely afresh (see also Ueda et al. 2003).

The spectral fitting shows that, after accounting for the effects of absorption in the few objects that require it, the objects in our sample are all consistent with a single power-law slope, which has a mean of

$\Gamma = 1.76 \pm 0.08$. This can be compared, for example, to the intrinsic spectrum of local Seyfert galaxies observed by *Ginga*, $\Gamma = 1.95 \pm 0.05$ or *ASCA*, $\Gamma = 1.91 \pm 0.07$ (Nandra & Pounds 1994; Nandra et al. 1997). These include the effects of both (sometimes ionized) absorption and X-ray 'Compton reflection'. While the former may be crudely accounted for in our fits, the latter is not. If Compton reflection is present in the *Chandra* spectra – which the spectral quality does not allow us to identify – then the intrinsic spectrum of the objects is likely to be steeper by $\Delta\Gamma \sim 0.1$. Arguably the cleanest comparison is with the *ASCA* Seyferts without accounting for reflection, which show $\Gamma = 1.79 \pm 0.07$, completely consistent with our derived *Chandra* mean. The existence of this 'canonical' X-ray spectrum (e.g. Turner & Pounds 1989) argues for a common emission process for the X-rays in the entire AGN population.

A final intriguing note is that the mean spectrum of the hard-band-selected sources is consistent with that expected from one dominated by Compton reflection (e.g. Matt et al. 1996, 2000). Thus a significant population of ultra-obscured AGNs is not ruled out, and indeed is supported by our analysis. Such objects are the likely origin of the peak in the XRB (Ueda et al. 2003; Worsley et al. 2004), which occurs at ∼30 keV (Marshall et al. 1980), and may make a significant contribution to the total discrete energy budget of the Universe (Fabian & Iwasawa 1999). The 75 per cent of our sample that is detected in the soft band, with typical $\Gamma = 1.9$, is likely to make a negligible contribution to the XRB peak unless the spectrum changes radically as a function of energy. It is therefore possible that – despite the extraordinary success of the *Chandra* deep surveys – the majority of the energy density in the XRB remains unresolved. The final mystery of the origin of the XRB therefore awaits deep surveys with a future, sensitive, hard X-ray telescope.

ACKNOWLEDGMENTS

This work has been supported by a *Chandra* grant awarded through SAO. We thank the *Chandra* X-ray Center for assistance with some analysis and software issues. ESL thanks PPARC for support in the form of a Research Studentship.

REFERENCES

Alexander D. M. et al., 2003, AJ, 126, 539 (A03)
Antonucci R. R. J., Miller J. S., 1985, ApJ, 297, 621
Barger A. J., Cowie L., Mushotzky R. F., Richards E. A., 2001, AJ, 121, 662
Barger A. J., Cowie L. L., Brandt W. N., Capak P., Garmire G. P., Hornschemeier A. E., Steffen A. T., Wehner E. H., 2002, AJ, 124, 1839
Bertin E., Arnouts S., 1996, A&AS, 117, 393
Blair A. J., Stewart G. C., Georgantopoulos I., Boyle B. J., Griffiths R. E., Shanks T., Almaini O., 2000, MNRAS, 314, L38
Brandt W. N. et al., 2001a, AJ, 122, 2810
Brandt W. N., Hornschemeier A. E., Scheider D. P., Alexander D. M., Bauer F. E., Garmire G. P., 2001b, ApJ, 558, L5
Comastri A., Setti G., Zamorani G., Hasinger G., 1995, A&A, 296, 1
Comastri A., Fiore F., Vignali C., Matt G., Perola G. C., La Franca F., 2001, MNRAS, 327, 781
Cowie L. L., Garmire G. P., Bautz M. W., Barger A. J., Brandt W. N., Hornschemeier A. E., 2002, ApJ, 566, L5
Cowie L. L., Barger A. J., Bautz M. W., Brandt W. N., Garmire G. P., 2003, ApJ, 584, L57
Davis M. et al., 2003, SPIE, 4834, 161
Dickey J. M., Lockman F. J., 1990, ARA&A, 28, 215
Eales S., Lilly S., Gear W., Dunne L., Bond R. J., Hammer F., Le Fèvre O., Crampton D., 1999, ApJ, 515, 518
Eales S., Lilly S., Webb T., Dunne L., Gear W., Clements D., Yun M., 2000, AJ, 120, 2244
Fabian A. C., Iwasawa K., 1999, MNRAS, 303, L34
Flores H. et al., 1999, ApJ, 517, 148
Fomalont E. A., Windhorst R. A., Kristian J. A., Kellerman K. I., 1991, AJ, 102, 1258
Freeman P. E., Kashyap V., Rosner R., Lamb D. Q., 2002, ApJS, 138, 185
Gehrels N., 1986, ApJ, 303, 336
Georgantopoulos I., Stewart G. C., Blair A. J., Shanks T., Griffiths R. E., Boyle B. J., Almaini O., Roche N., 1997, MNRAS, 291, 203
Georgantopoulos I., Georgakakis A., Akylas A., Stewart G. C., Giannakis O., Shanks T., Kitsionas S., 2004, MNRAS, 352, 91
Giacconi R. et al., 2001, ApJ, 551, 624
Giacconi R. et al., 2002, ApJS, 139, 369
Gilli R., Risaliti G., Salvati M., 1999, A&A, 347, 424
Gilli R., Salvati M., Hasinger G., 2001, A&A, 366, 407
Gilli R. et al., 2003, ApJ, 592, 721
Groth E. J., Kristian J. A., Lynds R. I., Earl J., Balsano R., Rhodes J., 1994, BAAS, 185, 5309
Kim D.-W. et al., 2004, ApJ, 600, 59
Lilly S. J., Tresse L., Hammer F., Crampton D., Le Fèvre O., 1995, ApJ, 455, 50
McCracken H. J., Le Fevre O., Brodwin M., Foucaud S., Lilly S. J., Crampton D., Mellier Y., 2001, A&A, 376, 756
Marshall F. E., Boldt E. A., Holt S. S., Miller R. B., Mushotzky R. F., Rose L. A., Rothschild R. E., Serlemitsos P. J., 1980, ApJ, 235, 4
Marshall H., Tennant A., Grant C. E., Hitchcock A. P., O'Dell S. L., Plucinsky P. P., 2004, SPIE, 5165, 497
Manners J. et al., 2003, MNRAS, 343, 293 (M03)
Matt G. et al., 1996, MNRAS, 280, L69
Matt G., Fabian A. C., Guainazzi M., Iwasawa K., Bassani L., Malaguti G., 2000, MNRAS, 318, 173
Miyaji T., Griffiths R. E., 2002, ApJ, 564, L5
Miyaji T., Sarajedini V., Griffiths R. E., Yamada T., Schurch M., Cristobal-Hornilos D., Motohara K., 2004, AJ, 127, 3180
Mushotzky R. F., Cowie L. L., Barger A. J., Arnaud K. A., 2000, Nat, 404, 459
Nandra K., Pounds K. A., 1994, MNRAS, 405, 268
Nandra K., George I. M., Mushotzky R. F., Turner T. J., Yaqoob T., 1997, ApJ, 477, 602
Nandra K., Mushotzky R. F., Arnaud K., Steidel C. C., Adelberger K. L., Gardner J. P., Teplitz H. I., Windhorst R. A., 2002, ApJ, 576, 625
Nandra K., Georgantopoulos I., Ptak A., Turner T. J., 2003, ApJ, 582, 615
Nandra K., Georgantopoulos I., Brotherton M., Papadakis I. E., 2004, MNRAS, 347, L41
Pappa A., Georgantopoulos I., Stewart G. C., Zezas A. L., 2001, MNRAS, 326, 995
Piconcelli E., Cappi M., Bassani L., Di Cocco G., Dadina M., 2003, A&A, 412, 689
Rosati P. et al., 2002, ApJ, 566, 667
Reynolds C. S., Fabian A. C., Makishima K., Fukazawa Y., Tamura T., 1994, MNRAS, 268, L55
Setti G., Woltjer L., 1989, A&A, 224, L21
Shanks T., Georgantopoulos I., Stewart G. C., Pounds K. A., Boyle B. J., Griffiths R. E., 1991, Nat, 353, 315
Steidel C. C., Adelberger K. L., Shapley A. E., Pettini M., Dickinson M., Giavalisco M., 2003, ApJ, 592, 728
Stern D. et al., 2002, AJ, 123, 2223
Tozzi P. et al., 2001, ApJ, 562, 42
Turner T. J., Pounds K. A., 1989, MNRAS, 240, 833
Ueda Y., Akiyama M., Ohta K., Miyaji T., 2003, ApJ, 598, 886
Wang J. X. et al., 2004, ApJ, 608, 21
Waskett T. et al., 2004, MNRAS, 350, 785
Webb T. M. A., Lilly S. J., Clements D. A., Eales S., Yun M., Brodwin M., Dunne L., Gear W. K., 2003, ApJ, 597, 680
Worsley M. A., Fabian A. C., Barcons X., Mateo S., Hasinger G., Brunner H., 2004, MNRAS, 352, L8
Yang Y., Mushotzky R. F., Barger A. J., Cowie L. L., Sanders D. B., Steffen A. T., 2003, ApJ, 585, L85

Table A1. Additional sources detected in ELAIS-N1. The columns are as follows: (1) source catalogue number; (2) *Chandra* object name; (3) full-band (0.5–7 keV) counts; (4) soft-band (0.5–2 keV) counts; (5) hard-band (2–7 keV) counts; (6) ultra-hard-band (4–7 keV) counts; (7) 0.5–10 keV flux (all fluxes 10^{-15} erg cm^{-2} s^{-1}); (8) 0.5–2 keV flux; (9) 2–10 keV flux; (10) 5–10 keV flux; (11) lowest false detection probability found for the four bands – a probability of 10^{-8} is assigned if the Poisson probability is less than this value; (12) off-axis angle in arcminutes; (13) hardness ratio = $(H - S)/(H + S)$, where H and S are the 2–7 keV and 0.5–2 keV counts, corrected to on-axis values; (14) fshu = source detected at $< 4 \times 10^{-6}$ probability in this band, where the bands are full (f), soft (s), hard (h) and ultra-hard (u) – the first band quoted is the one with the lowest probability (i.e. that quoted in column 11).

Cat. No. (1)	CXO EN1 (2000) (2)	FB counts (3)	SB counts (4)	HB counts (5)	UB counts (6)	0.5–10.0 flux (7)	0.5–2.0 flux (8)	2–10 flux (9)	5–10 flux (10)	$p_{\rm min}$ (11)	OAA (arcmin) (12)	HR (13)	Flags (14)
a6	J160929.1+542938	$12.9^{+5.3}_{-4.2}$	$5.5^{+4.0}_{-2.8}$	$6.7^{+4.3}_{-3.1}$	< 6.16	$3.60^{+1.10}_{-0.83}$	$0.40^{+0.20}_{-0.14}$	$2.90^{+1.20}_{-0.90}$	< 5.30	$10^{-6.1}$	8.30	0.1	f
a21	J160946.6+543008	$8.4^{+4.3}_{-3.1}$	$5.2^{+3.6}_{-2.4}$	< 5.00	< 4.30	$2.10^{+0.91}_{-0.66}$	$0.35^{+0.21}_{-0.14}$	< 1.90	< 3.20	$10^{-6.7}$	5.80	−1.0	sf
a39	J161001.9+544148	$7.9^{+4.8}_{-3.7}$	$8.1^{+4.4}_{-3.3}$	< 7.97	< 7.29	$2.10^{+0.72}_{-0.54}$	$0.56^{+0.23}_{-0.17}$	< 3.10	< 6.10	$10^{-5.6}$	8.90	−1.0	fs
a51	J161010.7+543556	$5.6^{+3.6}_{-2.4}$	< 2.82	$4.7^{+3.4}_{-2.2}$	< 3.75	$1.30^{+0.80}_{-0.53}$	< 0.18	$1.70^{+1.20}_{-0.74}$	< 2.50	$10^{-8.0}$	2.90	1.0	fh
a55	J161014.4+543359	$2.8^{+2.9}_{-1.6}$	< 2.90	$2.8^{+2.9}_{-1.6}$	< 2.86	$0.69^{+0.67}_{-0.37}$	< 0.19	$1.10^{+1.10}_{-0.58}$	< 2.00	$10^{-5.5}$	1.00	1.0	h
a61	J161017.5+543747	$4.2^{+3.4}_{-2.2}$	$3.7^{+3.2}_{-1.9}$	< 4.46	< 3.62	$1.00^{+0.69}_{-0.44}$	$0.23^{+0.19}_{-0.11}$	< 1.60	< 2.50	$10^{-5.8}$	4.40	−1.0	s
a62	J161018.2+543232	$3.7^{+3.2}_{-1.9}$	$3.9^{+3.2}_{-1.9}$	< 2.85	< 2.83	$0.87^{+0.69}_{-0.42}$	$0.24^{+0.19}_{-0.11}$	< 0.99	< 1.90	$10^{-5.7}$	0.90	−1.0	s
a69	J161020.7+544144	$12.8^{+5.3}_{-4.2}$	$10.8^{+4.7}_{-3.5}$	< 8.33	< 6.57	$3.30^{+0.99}_{-0.78}$	$0.74^{+0.27}_{-0.20}$	< 3.20	< 5.40	$10^{-6.1}$	8.40	−1.0	s
a76	J161026.0+543021	$7.6^{+4.0}_{-2.8}$	$5.7^{+3.6}_{-2.4}$	< 3.69	< 3.78	$1.80^{+0.91}_{-0.63}$	$0.37^{+0.22}_{-0.14}$	< 1.30	< 2.60	$10^{-8.0}$	3.10	−1.0	fs
a77	J161026.1+543253	$5.8^{+3.6}_{-2.4}$	$4.9^{+3.4}_{-2.2}$	< 2.84	< 2.86	$1.50^{+0.92}_{-0.61}$	$0.34^{+0.23}_{-0.15}$	< 1.10	< 2.30	$10^{-6.9}$	1.00	−1.0	f
a78	J161026.1+542528	$7.5^{+4.4}_{-3.3}$	$7.1^{+4.1}_{-2.9}$	< 6.80	< 5.70	$2.50^{+1.00}_{-0.74}$	$0.61^{+0.28}_{-0.20}$	< 3.40	< 5.90	$10^{-5.7}$	7.90	−1.0	s
a82	J161029.9+543315	$2.8^{+2.9}_{-1.6}$	$2.9^{+2.9}_{-1.6}$	< 2.82	< 2.85	$0.66^{+0.65}_{-0.36}$	$0.18^{+0.18}_{-0.10}$	< 1.00	< 2.10	$10^{-6.1}$	1.40	−1.0	s
a87	J161035.4+543558	$6.5^{+3.8}_{-2.6}$	$4.7^{+3.4}_{-2.2}$	< 3.66	< 3.73	$1.60^{+0.85}_{-0.58}$	$0.30^{+0.21}_{-0.13}$	< 1.30	< 2.70	$10^{-8.0}$	3.40	−1.0	fs
a88	J161037.2+542556	$10.6^{+5.0}_{-3.8}$	$5.7^{+4.0}_{-2.8}$	< 7.08	< 6.19	$3.10^{+1.00}_{-0.78}$	$0.43^{+0.21}_{-0.15}$	< 3.10	< 5.60	$10^{-5.6}$	7.80	−1.0	fs
a100	J161044.9+543003	$5.7^{+3.8}_{-2.6}$	$2.3^{+2.9}_{-1.6}$	$3.2^{+3.2}_{-1.9}$	< 4.40	$1.40^{+0.77}_{-0.53}$	$0.15^{+0.15}_{-0.08}$	$1.20^{+0.99}_{-0.59}$	< 3.30	$10^{-6.1}$	4.90	0.2	f
a103	J161045.9+543046	$5.7^{+3.8}_{-2.6}$	$3.3^{+3.2}_{-1.9}$	< 5.21	< 4.46	$1.40^{+0.77}_{-0.53}$	$0.22^{+0.17}_{-0.10}$	< 2.00	< 3.40	$10^{-6.1}$	4.50	−1.0	f
a114	J161048.8+543458	$5.1^{+3.6}_{-2.4}$	< 3.58	$4.3^{+3.4}_{-2.2}$	< 3.59	$1.30^{+0.76}_{-0.50}$	< 0.23	$1.70^{+1.20}_{-0.73}$	< 2.70	$10^{-6.2}$	4.50	1.0	fh
a125	J161056.3+543208	$4.5^{+3.6}_{-2.4}$	$4.1^{+3.4}_{-2.2}$	< 5.05	< 4.30	$1.10^{+0.68}_{-0.45}$	$0.28^{+0.19}_{-0.12}$	< 1.90	< 3.40	$10^{-5.5}$	5.40	−1.0	s
a137	J161111.6+543424	$15.4^{+5.6}_{-4.4}$	$6.0^{+4.0}_{-2.8}$	< 7.70	< 6.03	$4.10^{+1.10}_{-0.90}$	$0.42^{+0.21}_{-0.14}$	< 3.00	< 4.90	$10^{-5.8}$	7.50	−1.0	f
a140	J161116.5+543235	$14.0^{+5.7}_{-4.5}$	< 7.67	$10.5^{+5.0}_{-3.8}$	$6.3^{+4.1}_{-2.9}$	$3.90^{+1.10}_{-0.85}$	< 0.57	$4.60^{+1.50}_{-1.20}$	$5.90^{+2.70}_{-1.90}$	$10^{-6.6}$	8.20	1.0	hf
a142	J161120.6+543313	$8.4^{+4.4}_{-3.3}$	$5.7^{+3.8}_{-2.6}$	< 6.32	< 5.74	$7.70^{+3.10}_{-2.30}$	$1.40^{+0.74}_{-0.51}$	< 8.70	< 17.00	$10^{-5.6}$	8.80	−1.0	s

Table A2. Additional sources detected in HDF-N (see text). The columns are as follows: (1) source catalogue number; (2) *Chandra* object name; (3) full-band (0.5–7 keV) counts; (4) soft-band (0.5–2 keV) counts; (5) hard-band (2–7 keV) counts; (6) ultra-hard-band (4–7 keV) counts; (7) 0.5–10 keV flux (all fluxes 10^{-15} erg cm^{-2} s^{-1}); (8) 0.5–2 keV flux; (9) 2–10 keV flux; (10) 5–10 keV flux; (11) lowest false detection probability found for the four bands – a probability of 10^{-8} is assigned if the Poisson probability is less than this value; (12) off-axis angle in arcminutes; (13) hardness ratio = $(H - S)/(H + S)$, where H and S are the 2–7 keV and 0.5- 2 keV counts, corrected to on-axis values; (14) fshu = source detected at $< 4 \times 10^{-6}$ probability in this band, where the bands are full (f), soft (s), hard (h) and ultra-hard (u) – the first band quoted is the one with the lowest probability (i.e. that quoted in column 11).

Cat. No. (1)	CXO HDF-N (2000) (2)	FB counts (3)	SB counts (4)	HB counts (5)	UB counts (6)	0.5–10.0 flux (7)	0.5–2.0 flux (8)	2–10 flux (9)	5–10 flux (10)	$p_{\min}$ (11)	OAA (arcmin) (12)	HR (13)	Flags (14)
f9	J123523.2+621302	$65.5^{+11.9}_{-10.9}$	$40.8^{+9.1}_{-8.0}$	< 8.86	< 15.51	$6.50^{+0.66}_{-0.60}$	$1.10^{+0.15}_{-0.13}$	< 0.56	< 4.90	$10^{-8.0}$	9.90	−0.2	fs
f10	J123524.0+621359	$43.8^{+12.3}_{-11.2}$	$22.5^{+8.8}_{-7.7}$	$27.1^{+10.2}_{-9.1}$	< 15.51	$2.10^{+0.20}_{-0.19}$	$0.29^{+0.04}_{-0.04}$	$2.00^{+0.24}_{-0.22}$	< 2.30	$10^{-8.0}$	9.70	0.1	fh
f14	J123529.3+621223	$35.5^{+9.7}_{-8.6}$	$14.8^{+6.9}_{-5.8}$	$18.0^{+7.8}_{-6.7}$	< 13.55	$3.60^{+0.46}_{-0.41}$	$0.39^{+0.08}_{-0.07}$	$2.80^{+0.48}_{-0.42}$	< 4.30	$10^{-8.0}$	9.30	0.1	fs
f16	J123532.0+621458	$32.1^{+12.7}_{-11.7}$	< 13.55	$34.3^{+11.4}_{-10.4}$	< 13.55	$0.60^{+0.06}_{-0.05}$	< 0.07	$1.00^{+0.11}_{-0.10}$	< 0.79	$10^{-5.5}$	8.80	1.0	h
f17	J123532.4+621120	$19.5^{+8.3}_{-7.2}$	$19.9^{+6.9}_{-5.8}$	< 16.18	< 13.14	$2.60^{+0.41}_{-0.35}$	$0.70^{+0.14}_{-0.12}$	< 3.10	< 5.40	$10^{-5.5}$	9.20	−1.0	s
f41	J123551.8+620939	$22.7^{+7.6}_{-6.5}$	< 10.99	$18.7^{+6.8}_{-5.7}$	$10.4^{+5.4}_{-4.3}$	$2.40^{+0.43}_{-0.37}$	< 0.31	$3.10^{+0.63}_{-0.53}$	$3.50^{+1.00}_{-0.80}$	$10^{-5.7}$	7.90	1.0	hf
f42	J123552.5+622227	$21.0^{+7.8}_{-6.8}$	$18.6^{+6.4}_{-5.3}$	< 15.02	< 11.24	$2.90^{+0.49}_{-0.42}$	$0.68^{+0.15}_{-0.12}$	< 3.00	< 4.70	$10^{-5.9}$	10.50	−1.0	s
f49	J123555.1+620843	$30.9^{+8.4}_{-7.3}$	< 11.46	$23.6^{+7.4}_{-6.3}$	< 11.91	$3.40^{+0.53}_{-0.46}$	< 0.34	$4.00^{+0.74}_{-0.63}$	< 4.00	$10^{-6.7}$	8.20	1.0	f
f50	J123555.3+620835	$23.7^{+8.1}_{-7.0}$	< 11.66	$24.1^{+7.5}_{-6.4}$	< 11.91	$2.60^{+0.42}_{-0.36}$	< 0.34	$4.00^{+0.72}_{-0.61}$	< 3.90	$10^{-8.0}$	8.20	1.0	hf
f60	J123558.0+621354	$31.1^{+10.4}_{-9.4}$	$17.1^{+7.8}_{-6.8}$	$19.2^{+8.9}_{-7.8}$	$19.5^{+7.9}_{-6.8}$	$0.40^{+0.05}_{-0.04}$	$0.06^{+0.01}_{-0.01}$	$0.38^{+0.05}_{-0.05}$	$0.80^{+0.14}_{-0.12}$	$10^{-8.0}$	5.80	0.1	fs
f66	J123600.5+621215	$25.4^{+9.9}_{-8.8}$	< 17.68	$35.4^{+9.7}_{-8.6}$	$28.1^{+8.4}_{-7.3}$	$0.32^{+0.04}_{-0.04}$	< 0.06	$0.70^{+0.09}_{-0.08}$	$1.10^{+0.18}_{-0.16}$	$10^{-8.0}$	5.80	1.0	hfu
f74	J123604.7+622208	$22.4^{+10.6}_{-9.5}$	$22.5^{+8.3}_{-7.2}$	< 17.59	< 17.95	$0.57^{+0.07}_{-0.06}$	$0.15^{+0.02}_{-0.02}$	< 0.66	< 1.40	$10^{-6.5}$	9.40	−1.0	s
f91	J123608.8+621113	$16.0^{+8.6}_{-7.5}$	$14.8^{+7.1}_{-6.0}$	< 18.50	< 15.71	$0.22^{+0.03}_{-0.03}$	$0.05^{+0.01}_{-0.01}$	< 0.37	< 0.66	$10^{-7.2}$	5.40	−1.0	s
f93	J123610.2+620748	$21.2^{+8.2}_{-7.1}$	< 13.27	$16.9^{+7.2}_{-6.1}$	$11.4^{+6.0}_{-4.9}$	$1.30^{+0.21}_{-0.18}$	< 0.22	$1.60^{+0.30}_{-0.25}$	$2.20^{+0.55}_{-0.45}$	$10^{-6.2}$	7.70	1.0	h
f107	J123614.1+622523	$65.6^{+11.8}_{-10.8}$	< 16.17	$54.3^{+10.4}_{-9.3}$	$26.1^{+7.8}_{-6.7}$	$6.60^{+0.67}_{-0.61}$	< 0.43	$8.40^{+1.00}_{-0.90}$	$8.90^{+1.50}_{-1.30}$	$10^{-8.0}$	11.90	1.0	fhu
f112	J123615.1+621008	$30.9^{+9.6}_{-8.6}$	$9.2^{+6.6}_{-5.4}$	$17.6^{+8.1}_{-7.0}$	< 15.39	$0.38^{+0.05}_{-0.04}$	$0.03^{+0.01}_{-0.01}$	$0.34^{+0.06}_{-0.05}$	< 0.58	$10^{-7.2}$	5.50	0.3	f
f121	J123618.3+621550	$29.2^{+8.8}_{-7.7}$	$19.5^{+7.1}_{-6.1}$	$10.8^{+6.7}_{-5.6}$	< 13.62	$0.35^{+0.05}_{-0.04}$	$0.06^{+0.01}_{-0.01}$	$0.20^{+0.04}_{-0.04}$	< 0.49	$10^{-8.0}$	3.80	−0.3	f
f128	J123620.3+622507	$20.3^{+12.7}_{-11.6}$	$23.8^{+9.5}_{-8.5}$	< 10.54	< 10.54	$0.75^{+0.07}_{-0.06}$	$0.23^{+0.03}_{-0.03}$	< 0.57	< 1.20	$10^{-5.7}$	11.40	−1.0	s
f136	J123621.8+621323	$12.9^{+6.2}_{-5.1}$	< 10.28	$10.1^{+5.6}_{-4.4}$	$5.8^{+4.7}_{-3.5}$	$0.23^{+0.05}_{-0.04}$	< 0.05	$0.28^{+0.08}_{-0.06}$	$0.32^{+0.12}_{-0.09}$	$10^{-8.0}$	3.10	1.0	fh
f139	J123622.1+620517	$16.4^{+7.7}_{-6.6}$	$13.6^{+6.1}_{-5.0}$	< 15.25	< 12.33	$1.90^{+0.32}_{-0.28}$	$0.41^{+0.10}_{-0.08}$	< 2.50	< 4.30	$10^{-6.1}$	9.30	−1.0	s
f159	J123627.2+622231	$36.2^{+11.5}_{-10.5}$	< 9.60	$32.4^{+10.1}_{-9.0}$	$18.1^{+8.0}_{-6.9}$	$0.74^{+0.08}_{-0.07}$	< 0.05	$1.00^{+0.12}_{-0.11}$	$1.20^{+0.19}_{-0.17}$	$10^{-7.2}$	8.70	1.0	fh
f163	J123627.8+621448	$12.3^{+6.1}_{-5.0}$	< 9.82	$5.7^{+5.1}_{-4.0}$	$1.1^{+4.1}_{-2.9}$	$0.15^{+0.04}_{-0.03}$	< 0.03	$0.11^{+0.03}_{-0.03}$	$0.04^{+0.02}_{-0.01}$	$10^{-8.0}$	2.40	1.0	fh
f177	J123630.3+621332	< 11.35	$6.3^{+4.4}_{-3.3}$	< 10.13	< 9.70	< 0.13	$0.02^{+0.01}_{-0.01}$	< 0.18	< 0.34	$10^{-6.1}$	2.10	−1.0	s

Table A2 – *continued*

Cat. No. (1)	CXO HDF-N (2000) (2)	FB counts (3)	SB counts (4)	HB counts (5)	UB counts (6)	0.5–10.0 flux (7)	0.5–2.0 flux (8)	2–10 flux (9)	5–10 flux (10)	$p_{\rm min}$ (11)	OAA (arcmin) (12)	HR (13)	Flags (14)
f183	J123632.4+621104	$15.6^{+6.4}_{-5.3}$	$6.9^{+4.7}_{-3.5}$	< 12.20	< 10.41	$0.19^{+0.04}_{-0.04}$	$0.02^{+0.01}_{-0.01}$	< 0.22	< 0.37	$10^{-6.6}$	3.50	−1.0	fs
f188	J123633.3+621408	$14.6^{+5.9}_{-4.8}$	$11.4^{+5.1}_{-4.0}$	< 4.71	< 9.05	$0.17^{+0.04}_{-0.04}$	$0.04^{+0.01}_{-0.01}$	< 0.03	< 0.32	$10^{-7.2}$	1.70	−0.3	f
f193	J123633.8+622039	$54.8^{+12.3}_{-11.2}$	$21.2^{+8.7}_{-7.6}$	$39.6^{+10.6}_{-9.5}$	< 17.51	$0.82^{+0.08}_{-0.07}$	$0.09^{+0.01}_{-0.01}$	$0.91^{+0.11}_{-0.09}$	< 0.78	$10^{-8.0}$	6.70	0.3	fh
f206	J123636.0+622729	$37.9^{+13.2}_{-12.1}$	$39.5^{+10.4}_{-9.4}$	< 9.59	< 9.59	$2.30^{+0.21}_{-0.19}$	$0.65^{+0.08}_{-0.07}$	< 0.89	< 2.00	$10^{-5.7}$	13.40	−1.0	s
f213	J123637.3+622546	$80.8^{+18.7}_{-17.6}$	< 16.26	$59.5^{+15.7}_{-14.7}$	< 16.26	$1.80^{+0.11}_{-0.10}$	< 0.09	$2.00^{+0.15}_{-0.14}$	< 1.10	$10^{-6.9}$	11.70	1.0	fh
f214	J123637.9+621116	$13.8^{+6.2}_{-5.1}$	$7.5^{+4.7}_{-3.5}$	< 10.95	< 10.19	$0.16^{+0.04}_{-0.03}$	$0.02^{+0.01}_{-0.01}$	< 0.19	< 0.36	$10^{-7.2}$	3.10	−1.0	sf
f219	J123639.2+621656	$10.3^{+6.3}_{-5.2}$	$11.2^{+5.6}_{-4.4}$	< 13.09	< 11.36	$0.13^{+0.03}_{-0.03}$	$0.04^{+0.01}_{-0.01}$	< 0.25	< 0.43	$10^{-5.9}$	3.00	−1.0	s
f230	J123641.1+622412	$79.0^{+15.8}_{-14.8}$	$21.0^{+10.0}_{-8.9}$	$57.1^{+13.4}_{-12.4}$	< 14.15	$1.70^{+0.12}_{-0.11}$	$0.12^{+0.02}_{-0.01}$	$1.90^{+0.17}_{-0.15}$	< 0.95	$10^{-8.0}$	10.10	0.5	fh
f240	J123643.2+621626	$10.8^{+5.9}_{-4.8}$	< 5.33	< 11.15	< 10.22	$0.15^{+0.04}_{-0.03}$	< 0.01	< 0.23	< 0.44	$10^{-5.6}$	2.40	−1.0	f
f246	J123644.4+622556	$98.1^{+20.3}_{-19.2}$	< 9.46	$98.5^{+17.8}_{-16.8}$	$45.3^{+13.4}_{-12.3}$	$2.20^{+0.12}_{-0.11}$	< 0.06	$3.40^{+0.21}_{-0.20}$	$3.40^{+0.30}_{-0.28}$	$10^{-8.0}$	11.80	1.0	fh
f247	J123644.8+621715	< 5.97	$12.1^{+5.6}_{-4.4}$	< 12.86	< 10.66	< 0.03	$0.05^{+0.01}_{-0.01}$	< 0.29	< 0.50	$10^{-5.4}$	3.10	−1.0	s
f249	J123645.1+621106	$14.7^{+6.2}_{-5.1}$	$11.6^{+5.2}_{-4.1}$	< 10.63	< 9.84	$0.19^{+0.04}_{-0.04}$	$0.04^{+0.01}_{-0.01}$	< 0.20	< 0.37	$10^{-6.4}$	3.00	−1.0	f
f253	J123645.3+621522	$12.5^{+5.7}_{-4.5}$	$13.6^{+5.3}_{-4.2}$	< 10.30	< 9.47	$0.15^{+0.04}_{-0.03}$	$0.04^{+0.01}_{-0.01}$	< 0.18	< 0.34	$10^{-5.7}$	1.30	−1.0	f
f255	J123645.4+621127	$10.1^{+5.6}_{-4.4}$	$12.7^{+5.2}_{-4.1}$	< 9.89	< 9.45	$0.13^{+0.04}_{-0.03}$	$0.04^{+0.01}_{-0.01}$	< 0.18	< 0.35	$10^{-8.0}$	2.70	−1.0	s
f257	J123645.9+620833	$20.8^{+9.1}_{-8.0}$	< 15.78	$14.6^{+7.8}_{-6.8}$	< 16.10	$0.26^{+0.04}_{-0.03}$	< 0.05	$0.28^{+0.05}_{-0.04}$	< 0.60	$10^{-6.9}$	5.60	1.0	fh
f263	J123646.5+621048	$10.5^{+5.9}_{-4.8}$	$6.2^{+4.6}_{-3.4}$	< 11.03	< 10.29	$0.14^{+0.04}_{-0.03}$	$0.02^{+0.01}_{-0.01}$	< 0.22	< 0.42	$10^{-8.0}$	3.30	−1.0	sf
f266	J123647.5+621639	$8.1^{+5.4}_{-4.3}$	< 9.19	$14.3^{+5.8}_{-4.7}$	< 9.11	$0.13^{+0.04}_{-0.03}$	< 0.04	$0.36^{+0.10}_{-0.08}$	< 0.45	$10^{-6.1}$	2.50	1.0	h
f272	J123648.3+620246	$71.9^{+13.3}_{-12.3}$	$49.1^{+10.0}_{-9.0}$	< 9.53	< 9.53	$5.00^{+0.44}_{-0.41}$	$0.91^{+0.11}_{-0.10}$	< 0.97	< 2.10	$10^{-8.0}$	11.40	−1.0	fs
f273	J123648.6+620444	$61.0^{+13.6}_{-12.6}$	$62.0^{+11.5}_{-10.4}$	< 9.53	< 9.53	$1.80^{+0.15}_{-0.14}$	$0.48^{+0.05}_{-0.05}$	< 0.40	< 0.85	$10^{-8.0}$	9.40	−1.0	sf
f282	J123650.1+621239	$14.4^{+5.8}_{-4.7}$	< 6.93	< 9.11	< 8.93	$0.17^{+0.04}_{-0.04}$	< 0.02	< 0.16	< 0.31	$10^{-5.6}$	1.50	...	f
f287	J123651.2+621551	$12.7^{+5.7}_{-4.5}$	$9.6^{+4.8}_{-3.7}$	< 10.10	< 9.37	$0.15^{+0.04}_{-0.03}$	$0.03^{+0.01}_{-0.01}$	< 0.18	< 0.34	$10^{-5.6}$	1.80	−1.0	s
f302	J123653.9+621503	$12.4^{+5.6}_{-4.4}$	$4.2^{+3.8}_{-2.6}$	$8.0^{+4.7}_{-3.5}$	< 8.32	$0.15^{+0.04}_{-0.03}$	$0.01^{+0.01}_{0.00}$	$0.15^{+0.05}_{-0.04}$	< 0.30	$10^{-5.8}$	1.20	0.3	f
f303	J123653.9+621045	< 6.07	$6.3^{+4.8}_{-3.7}$	< 12.82	< 11.07	< 0.02	$0.02^{+0.01}_{-0.01}$	< 0.22	< 0.39	$10^{-5.5}$	3.40	−1.0	s
f321	J123657.8+620826	$20.2^{+9.8}_{-8.7}$	$16.2^{+7.5}_{-6.4}$	< 12.03	< 17.28	$0.25^{+0.03}_{-0.03}$	$0.05^{+0.01}_{-0.01}$	< 0.22	< 0.65	$10^{-6.1}$	5.80	−1.0	s
f369	J123707.8+621056	$16.9^{+8.2}_{-7.1}$	$24.8^{+7.2}_{-6.1}$	< 16.02	< 13.53	$0.20^{+0.03}_{-0.03}$	$0.08^{+0.02}_{-0.01}$	< 0.28	< 0.48	$10^{-7.2}$	4.00	−1.0	sf
f370	J123708.0+621658	$22.9^{+7.9}_{-6.8}$	$19.5^{+6.6}_{-5.5}$	< 14.83	< 12.67	$0.27^{+0.05}_{-0.04}$	$0.06^{+0.01}_{-0.01}$	< 0.26	< 0.44	$10^{-8.0}$	3.70	−1.0	sf

Table A2 – *continued*

Cat. No. (1)	CXO HDF-N (2000) (2)	FB counts (3)	SB counts (4)	HB counts (5)	UB counts (6)	0.5–10.0 flux (7)	0.5–2.0 flux (8)	2–10 flux (9)	5–10 flux (10)	$p_{\rm min}$ (11)	OAA (arcmin) (12)	HR (13)	Flags (14)
f372	J123708.3+621513	$15.4^{+6.4}_{-5.3}$	$6.1^{+4.6}_{-3.4}$	$9.7^{+5.4}_{-4.3}$	< 10.72	$0.19^{+0.04}_{-0.04}$	$0.02^{+0.01}_{-0.01}$	$0.18^{+0.05}_{-0.04}$	< 0.38	$10^{-6.1}$	2.70	0.2	f
f390	J123712.7+621545	$19.4^{+7.2}_{-6.1}$	$10.2^{+5.4}_{-4.3}$	< 13.45	< 11.25	$0.23^{+0.04}_{-0.04}$	$0.03^{+0.01}_{-0.01}$	< 0.23	< 0.39	$10^{-8.0}$	3.40	−1.0	sf
f414	J123718.7+621314	< 15.48	$6.3^{+5.0}_{-3.8}$	< 13.22	< 10.89	< 0.25	$0.03^{+0.01}_{-0.01}$	< 0.31	< 0.51	$10^{-6.3}$	3.70	−1.0	s
f417	J123719.8+621336	$20.3^{+7.5}_{-6.4}$	< 11.86	$17.0^{+6.8}_{-5.7}$	$12.4^{+5.9}_{-4.8}$	$0.28^{+0.05}_{-0.04}$	< 0.04	$0.37^{+0.08}_{-0.06}$	$0.54^{+0.14}_{-0.11}$	$10^{-5.6}$	3.80	1.0	u
f444	J123727.1+621022	$26.7^{+11.3}_{-10.2}$	< 16.63	$23.9^{+10.0}_{-8.9}$	$24.4^{+8.8}_{-7.7}$	$0.34^{+0.04}_{-0.03}$	< 0.06	$0.47^{+0.06}_{-0.05}$	$1.00^{+0.15}_{-0.13}$	$10^{-5.7}$	5.90	1.0	u
f445	J123727.6+620857	$15.6^{+9.0}_{-7.9}$	$16.0^{+7.5}_{-6.4}$	< 16.63	< 16.52	$0.44^{+0.06}_{-0.05}$	$0.12^{+0.02}_{-0.02}$	< 0.69	< 1.40	$10^{-5.5}$	7.00	−1.0	s
f448	J123729.9+621300	$11.9^{+8.9}_{-7.8}$	$17.1^{+7.5}_{-6.4}$	< 16.12	< 17.09	$0.15^{+0.02}_{-0.02}$	$0.06^{+0.01}_{-0.01}$	< 0.30	< 0.64	$10^{-5.4}$	5.10	−1.0	s
f454	J123732.0+620335	$15.5^{+7.4}_{-6.3}$	$12.9^{+6.0}_{-4.9}$	< 14.56	< 11.58	$2.70^{+0.49}_{-0.42}$	$0.58^{+0.14}_{-0.12}$	< 3.70	< 6.40	$10^{-6.2}$	11.80	−1.0	s
f455	J123732.2+621303	$35.2^{+10.6}_{-9.6}$	$30.7^{+8.6}_{-7.5}$	< 11.58	< 17.32	$0.44^{+0.05}_{-0.05}$	$0.10^{+0.02}_{-0.01}$	< 0.21	< 0.64	$10^{-6.7}$	5.30	−1.0	s
f459	J123734.4+622326	$52.4^{+14.9}_{-13.8}$	$39.4^{+10.8}_{-9.7}$	$18.9^{+11.6}_{-10.6}$	< 13.05	$2.20^{+0.17}_{-0.16}$	$0.44^{+0.05}_{-0.04}$	$1.30^{+0.13}_{-0.12}$	< 1.90	$10^{-6.3}$	10.80	−0.3	f
f464	J123735.4+621055	$54.6^{+12.9}_{-11.9}$	$35.0^{+9.8}_{-8.8}$	< 18.68	< 18.68	$0.79^{+0.07}_{-0.07}$	$0.13^{+0.02}_{-0.02}$	< 0.40	< 0.82	$10^{-6.1}$	6.40	−1.0	f
f474	J123738.5+621702	< 19.28	$22.7^{+9.1}_{-8.0}$	< 19.28	< 19.28	< 0.26	$0.08^{+0.01}_{-0.01}$	< 0.38	< 0.78	$10^{-5.9}$	6.60	−1.0	s
f479	J123740.8+621231	$38.0^{+12.6}_{-11.5}$	$25.5^{+9.6}_{-8.5}$	< 19.28	< 19.28	$0.48^{+0.04}_{-0.04}$	$0.09^{+0.01}_{-0.01}$	< 0.36	< 0.73	$10^{-6.3}$	6.40	−1.0	s
f483	J123741.8+620617	$42.4^{+11.7}_{-10.7}$	< 18.66	$31.4^{+10.0}_{-9.0}$	< 18.63	$1.70^{+0.17}_{-0.16}$	< 0.19	$2.00^{+0.24}_{-0.22}$	< 2.40	$10^{-5.6}$	10.10	1.0	f
f490	J123745.3+620927	$21.1^{+8.5}_{-7.5}$	< 14.45	< 17.26	< 13.94	$0.72^{+0.11}_{-0.10}$	< 0.13	< 0.88	< 1.50	$10^{-5.5}$	8.20	...	f
f501	J123755.6+621507	$164.4^{+19.4}_{-18.4}$	$158.5^{+16.9}_{-15.9}$	$32.0^{+12.9}_{-11.9}$	< 18.65	$2.20^{+0.13}_{-0.12}$	$0.57^{+0.04}_{-0.04}$	$0.66^{+0.06}_{-0.05}$	< 0.76	$10^{-8.0}$	8.00	−0.6	fs
f504	J123758.6+621643	$45.7^{+18.5}_{-17.4}$	$15.1^{+13.4}_{-12.3}$	< 14.52	< 18.65	$0.62^{+0.04}_{-0.04}$	$0.05^{+0.00}_{0.00}$	< 0.03	< 0.77	$10^{-5.5}$	8.70	0.2	f
f509	J123801.0+621111	$49.2^{+11.7}_{-10.7}$	$40.6^{+9.8}_{-8.8}$	< 18.65	< 17.31	$1.70^{+0.17}_{-0.16}$	$0.37^{+0.05}_{-0.04}$	< 0.95	< 1.90	$10^{-8.0}$	9.00	−1.0	fs
f512	J123804.0+621006	$36.2^{+11.4}_{-10.3}$	< 17.31	$33.8^{+10.0}_{-9.0}$	< 18.02	$1.30^{+0.14}_{-0.13}$	< 0.17	$1.90^{+0.24}_{-0.21}$	< 2.10	$10^{-6.0}$	9.80	1.0	h
f519	J123816.2+620904	$44.5^{+12.4}_{-11.3}$	$21.5^{+9.1}_{-8.0}$	$22.2^{+9.6}_{-8.6}$	< 17.42	$2.40^{+0.23}_{-0.21}$	$0.31^{+0.04}_{-0.04}$	$1.90^{+0.24}_{-0.22}$	< 3.10	$10^{-8.0}$	11.50	0.1	f
f522	J123817.8+620857	$54.8^{+12.1}_{-11.1}$	$32.3^{+9.4}_{-8.3}$	$22.9^{+9.1}_{-8.0}$	< 17.06	$3.90^{+0.38}_{-0.35}$	$0.60^{+0.08}_{-0.07}$	$2.50^{+0.36}_{-0.32}$	< 4.00	$10^{-8.0}$	11.70	−0.1	fs
f524	J123819.9+620934	$46.5^{+12.5}_{-11.5}$	$27.6^{+9.5}_{-8.5}$	< 17.06	< 17.06	$2.50^{+0.23}_{-0.21}$	$0.39^{+0.05}_{-0.05}$	< 1.30	< 3.00	$10^{-5.7}$	11.70	−1.0	fs
f529	J123826.9+621545	$66.7^{+16.6}_{-15.6}$	< 17.81	$57.6^{+14.3}_{-13.3}$	< 17.81	$2.60^{+0.18}_{-0.17}$	< 0.19	$3.50^{+0.28}_{-0.26}$	< 2.20	$10^{-5.6}$	11.70	1.0	f
f531	J123827.8+621631	$70.2^{+17.0}_{-15.9}$	$29.7^{+10.8}_{-9.7}$	$43.0^{+14.1}_{-13.0}$	< 8.81	$2.80^{+0.19}_{-0.18}$	$0.32^{+0.04}_{-0.03}$	$2.70^{+0.22}_{-0.21}$	< 1.20	$10^{-7.2}$	11.90	0.2	f
f532	J123830.1+621019	$28.3^{+11.0}_{-9.9}$	$30.2^{+9.1}_{-8.0}$	< 8.81	< 17.44	$2.20^{+0.24}_{-0.22}$	$0.62^{+0.09}_{-0.08}$	< 1.00	< 4.40	$10^{-8.0}$	12.60	−1.0	sf
f536	J123842.5+621143	$69.6^{+13.5}_{-12.5}$	$57.0^{+10.9}_{-9.8}$	< 16.53	< 19.05	$5.30^{+0.46}_{-0.42}$	$1.20^{+0.13}_{-0.12}$	< 1.90	< 4.80	$10^{-8.0}$	13.60	−1.0	fs

APPENDIX A: SOURCE DETECTION IN HDF-N AND ELAIS-N1 FIELDS

As described above, in order to make a fair comparison between the number counts in the GWS with other fields, we have applied our source detection technique to two comparison fields, ELAIS-N1 (Manners et al. 2003) and the 2 Ms HDF-N survey (Alexander et al. 2003). For completeness, we describe the results of our analysis in more detail here, and compare them to the previous work.

A1 ELAIS-N1

As stated above, applying our analysis method to the ELAIS-N1 data resulted in 145 band-merged sources, with 132 FB, 116 SB, 88 HB and 29 UB. For comparison, in the published catalogue of M03 there are 124 band-merged ACIS-I sources (i.e. excluding six ACIS-S sources identified by M03; we do not consider the S chips in our analysis). Matching the two source lists shows that we identify all the M03 sources, but detect 21 additional sources. These extra sources are shown in Table A1. They were visually inspected to ensure that they were likely to be real and not artefacts.

There are a number of differences in the analyses presented by M03 and us. M03 used the pipeline-processed EVT2 files, whereas we used our own processing. We have filtered out background flares, so our exposure time of 70.0 ks is shorter than the 71.2 ks of M03. They performed source detection on the binned image, whereas we use the raw one. Finally, we adopted an upper limit of 7 keV whereas their source detection used the data up to 8 keV. Given the fact that we detect all the ACIS-I sources in M03 and 21 additional sources, we are confident that our procedure has resulted in a more comprehensive point-source catalogue in the case of ELAIS-N1.

A2 HDF-N

Running our source procedure at a threshold of 4×10^{-6} on the 2 Ms exposure of the HDF-N resulted in 536 band-merged sources. There are 485 FB, 432 SB, 312 HB and 187 UB sources. Matching this to the main catalogue of Alexander et al. (2003), which contains 503 sources, gives 461 sources in common. We detect 75 sources that A03 do not, and these are listed in Table A2. A03 detect 42 sources that are not significant in our analysis. We note that our analysis does not necessarily cast doubt on the reality of these 42 sources – weak and slightly extended sources could be missed by our method, and we use circular aperture extraction rather than the true PSF shape. It is highly likely, however, that the additional 75 sources we detect that A03 do not are also real. A large fraction ($\sim$40 per cent) of the non-common sources are close to the chip edges or the chip gaps, where any detection procedure will have difficulty and produce mixed results.

Again there are differences between our basic analysis and that of A03, which can also account for the differences in the source lists. Our screening was slightly more stringent (1.86 Ms exposure versus 1.95 Ms in A03), and A03 used an upper bound of 8 keV, rather than 7 keV. They also performed source detection in a total of seven bands, not four, and repeated the analysis for the restricted ACIS grade set, as well as the standard *ASCA* grade set we use here.

This paper has been typeset from a TEX/LATEX file prepared by the author.